nature microbiology

Article

https://doi.org/10.1038/s41564-024-01599-9

Inactive hydrothermal vent microbial communities are important contributors to deep ocean primary productivity

Received: 19 July 2023

Accepted: 20 December 2023

Published online: 29 January 2024



Amanda M. Achberger ®¹ ⊠, Rose Jones², John Jamieson³, Charles P. Holmes II¹, Florence Schubotz ®⁴, Nicolette R. Meyer⁵, Anne E. Dekas ®⁵, Sarah Moriarty³, Eoghan P. Reeves⁶, Alex Manthey⁴, Jonas Brünjes ®⁴, Daniel J. Fornari⁶, Margaret K. Tivey⁶, Brandy M. Toner² & Jason B. Sylvan ®¹⊠

Active hydrothermal vents are oases for productivity in the deep ocean, but the flow of dissolved substrates that fuel such abundant life ultimately ceases, leaving behind inactive mineral deposits. The rates of microbial activity on these deposits are largely unconstrained. Here we show primary production occurs on inactive hydrothermal deposits and quantify its contribution to new organic carbon production in the deep ocean. Measured incorporation of ¹⁴C-bicarbonate shows that microbial communities on inactive deposits fix inorganic carbon at rates comparable to those on actively venting deposits. Single-cell uptake experiments and nanoscale secondary ion mass spectrometry showed chemoautotrophs comprise a large fraction (>30%) of the active microbial cells. Metagenomic and lipidomic surveys of inactive deposits further revealed that the microbial communities are dominated by Alphaproteobacteria and Gammaproteobacteria using the Calvin-Benson-Bassham pathway for carbon fixation. These findings establish inactive vent deposits as important sites for microbial activity and organic carbon production on the seafloor.

Venting of hydrothermal fluid occurs primarily at globally distributed sites along approximately 89,000 km of mid-ocean ridges (MORs), back-arc spreading centres and volcanic arcs¹. Mixing of this reduced, metal and hydrogen-sulfide-rich fluid with oxygenated seawater results in precipitation and accumulation of primarily sulfide and sulfate minerals in the form of hydrothermal chimney deposits and provides an energy-rich habitat to support abundant and diverse chemosynthetic-based ecosystems²⁻⁵. While venting of hydrothermal

fluids can persist at some locations for thousands of years⁶⁻⁸, venting activity is spatially and temporally localized resulting in an as yet undetermined, but likely large, volumes of inactive hydrothermal mineral deposits along the crests and rift valleys of the global MOR. These inactive hydrothermal deposits can endure on the seafloor as small chimney-like features or as larger seafloor massive sulfide (SMS) accumulations for at least tens of thousands of years post venting^{7,9-12}. Current best estimates suggest the global mass of SMS deposits could

¹Department of Oceanography, Texas A&M University, College Station, Texas, USA. ²Department of Soil, Water and Climate, University of Minnesota-Twin Cities, St Paul, MN, USA. ³Department of Earth Sciences, Memorial University of Newfoundland, St John's, Newfoundland and Labrador, Canada. ⁴MARUM Center for Marine Environmental Sciences, University of Bremen, Bremen, Germany. ⁵Department of Earth System Science, Stanford University, Stanford, CA, USA. ⁶Department of Earth Science, Centre for Deep Sea Research, University of Bergen, Bergen, Norway. ⁷Department of Earth Sciences, University of Toronto, Toronto, Ontario, Canada. ⁸Department of Geology and Geophysics, Woods Hole Oceanographic Institution, Woods Hole, MA, USA. ⁹Department of Marine Chemistry and Geochemistry, Woods Hole Oceanographic Institution, Woods Hole, MA, USA. ⁸Department of Marine Chemistry and Geochemistry, Woods Hole Oceanographic Institution, Woods Hole, MA, USA. ⁸Department of Marine Chemistry and Geochemistry, Woods Hole Oceanographic Institution, Woods Hole, MA, USA. ⁸Department of Marine Chemistry and Geochemistry, Woods Hole Oceanographic Institution, Woods Hole, MA, USA. ⁸Department of Marine Chemistry and Geochemistry, Woods Hole Oceanographic Institution, Woods Hole, MA, USA. ⁸Department of Marine Chemistry and Geochemistry, Woods Hole Oceanographic Institution, Woods Hole, MA, USA. ⁸Department of Marine Chemistry and Geochemistry, Woods Hole Oceanographic Institution, Woods Hole, MA, USA. ⁸Department of Marine Chemistry and Geochemistry, Woods Hole Oceanographic Institution, Woods Hole, MA, USA. ⁸Department of Marine Chemistry and Geochemistry, Woods Hole, MA, USA. ⁸Department of Marine Chemistry and Geochemistry, Woods Hole, MA, USA. ⁸Department of Marine Chemistry and Geochemistry, Woods Hole, MA, USA. ⁸Department of Marine Chemistry and Geochemistry and Marine Chemistry and Marine Chem

be on the order of 10^8 tons¹, and, in some regions, these minerals may contain high enough concentrations of commercially important metals (for example, Cu, Zn, Au and Ag) to make them economically viable targets for seafloor mining activity¹³.

Following the cessation of high-temperature venting, organisms reliant on the flow of energy-rich substrates in hydrothermal fluid can no longer persist, leading to a shift in the composition of the animal and microbial communities ^{14–16}. While inactive hydrothermal deposits typically lack the abundant macro-faunal life associated with their actively venting counterparts, studies have shown that they do host densely populated and diverse microbial communities primarily supported by the abundant chemically reduced sulfur and iron species in the mineral deposits ^{14,17–21}. Typical members of this community include chemosynthetic Gammaproteobacteria and Alphaproteobacteria which can fix inorganic carbon via the Calvin–Benson–Bassham (CBB) cycle as well as Desulfobacterota and Nitrospirae, which utilize the reverse tricarboxylic acid cycle (rTCA) and the Wood–Ljungdahl (WL) pathway ^{16,18,22,23}. Heterotrophic species within the Bacteroidota are also commonly detected ^{14,16,18,22,23}.

While expanding genomic, proteomic and lipid-based studies of globally distributed inactive hydrothermal deposits has helped characterize the microbial community structure and its potential metabolic function, our understanding of the biogeochemical impact these organisms have on the deep-sea ecosystem is lagging, largely because we do not have quantitative assessments about their metabolic activity. Without such data, our understanding of inactive vents ecosystem elemental cycling and its potential influence on deep ocean biogeochemistry is incomplete. In addition, determining the ecosystem services provided by inactive hydrothermal deposits is critical for developing management and conservation strategies should these systems be exploited by deep-sea mining efforts^{24,25}.

In this Article, we use bulk and single-cell approaches to examine rates of primary productivity by hydrothermal mineral-hosted microbial communities collected from active and inactive vent deposits at the East Pacific Rise (EPR) crest near 9° 50′ N (Fig. 1), one of the best studied MOR vent systems representing fast-spreading lithosphere (for example, ref. 26). We further use metagenomic and isotopic analyses to assess the microbiome structure of the inactive hydrothermal deposits and evaluate the prevalence of various inorganic carbon fixation pathways utilized by the chemosynthetic population. Our measurements of primary production on inactive seafloor deposits begin to constrain the importance of these globally distributed biomes to the deep-sea ecosystem and ocean carbon budget.

Results

Sample characteristics

Samples of hydrothermal mineral deposits were collected from chimneys actively venting high-temperature fluids as well as inactive chimneys in proximity to (<20 m; hereafter named inactive-but-proximal) and distally located (>250 m) from detectable hydrothermal fluid flow (Extended Data Table 1). Most of the samples are dominated (>90% modal abundance) by a typical MOR hydrothermal sulfide mineral assemblage (for example, sphalerite, pyrite, marcasite, chalcopyrite and minor pyrrhotite) arranged in zonation patterns from the interior to the exterior (Extended Data Table 1 and Extended Data Fig. 1a). Anhydrite was frequently observed as a minor mineral phase in the active vent deposits but comprises >98% of sample BioVent 1. Anhydrite is also present in an inactive deposit sample (Mosh Pit 5) and an inactive-but-proximal sample (Bio95). Iron-oxyhydroxide and atacamite, which can form from oxidation of sulfide minerals, are common in the inactive hydrothermal deposits but rare in the active samples (Extended Data Fig. 1b). Four samples from inactive deposits (Mosh Pit and Lucky's Mound) were subdivided from the inner conduit to the outer surface (for example, Extended Data Fig. 1c). These subsamples show a substantial increase in overall Fe-oxyhydroxide and atacamite content towards the exterior of the samples, with some 'outer' subsamples consisting almost exclusively of Fe-oxyhydroxide (Extended Data Fig. 1b).

Carbon fixation activity on hydrothermal vent deposits

The deposits collected from various actively venting chimneys had statistically similar carbon fixation rates and an average rate of 1.38 nmol C g⁻¹ d⁻¹ (Fig. 2a and Table 1). The average carbon fixation rates were slightly higher for the inactive (3.32 nmol C g⁻¹ d⁻¹) and inactive-but-proximal (1.55 nmol C g⁻¹ d⁻¹) deposits but statistically the same (P = 0.46 and 0.30, respectively) as those measured from actively venting chimneys (Fig. 2a and Table 1). At the Bio9 and BioVent sites, samples from both active and inactive-but-proximal chimney types were collected. At these sites carbon fixation rates from the inactive-but-proximal deposits were nearly identical to their active counterparts (Fig. 2a). All three vent types showed a large variability in rates ranging over two orders of magnitude. There was no significant difference in cell concentrations between the vent types (P \geq 0.12; Extended Data Table 1), and carbon fixation rates normalized to total cell abundance were also statistically the same (Extended Data Fig. 2).

For the subdivided inactive hydrothermal deposit samples collected from Mosh Pit and Lucky's Mound, the average carbon fixation rate was greatest in the outermost, Fe-oxyhydroxide-rich layer at 26.6 nmol C g⁻¹ d⁻¹, followed by the inner, sulfide mineral-rich and Fe-oxyhydroxide-poor conduit at 0.26 nmol C g⁻¹ d⁻¹ (Fig. 2b and Extended Data Fig. 1b,c). The middle section could only be cleanly separated from the inner conduit in two of the four samples but showed the lowest rates (average = $0.08 \text{ nmol C g}^{-1} \text{ d}^{-1}$). The single fastest rate measured (74.8 nmol C g⁻¹ d⁻¹) was from an exterior portion of Lucky's Mound (Fig. 2b) which had a prominent (~1 mm thick) Fe-oxyhydroxide layer. Among all the samples, high carbon fixation rates frequently occurred in samples dominated by Fe-oxyhydroxide. Other sample characteristics (Extended Data Table 1), such as estimated porosity, relative abundance of specific sulfide minerals (Extended Data Fig. 1b) or distance from active venting, showed no correlation with fixation rates.

Single-cell activity measurements indicate chemoautotrophy

A complementary single-cell analysis of microbial anabolic activity and uptake of inorganic carbon in vent deposits was conducted at two additional sites: Alvinellid Rock (active) and M Vent (inactive; Figs. 1 and 3a). Anabolic activity, measured as uptake of ¹⁵N-ammonium and/or ¹³C-bicarbonate, was only detectable in a small percentage of the total microbial cell population in the samples from both the active and inactive vents investigated after 2 days (16% and 6%, respectively; Fig. 3b and Extended Data Fig. 3). However, this is considered a minimum estimate of active cells as both ex situ incubation conditions and conservative thresholds for detectable activity can result in underestimates. Within the active cell population, assimilation of inorganic carbon by chemoautotrophs was present. Chemoautotrophs were found to represent 49% and 31% of the total active cells in the active and inactive vent deposits, respectively, and were the most anabolically active cells (Fig. 3b and Extended Data Fig. 4).

Metagenomic insight into carbon fixation

Metagenomic analysis of the microbial communities present in representative inactive-but-proximal (Bio9) and inactive (Mosh Pit and Lucky's Mound) vent deposits (Fig. 1) were conducted to characterize the communities' diversity and genetic potential to fix inorganic carbon. Deposits at all three sites were primarily composed of Gammaproteobacteria and Alphaproteobacteria (Fig. 4a); however, differences were observed between the two vent types. The microbial communities found on the inactive-but-proximal Bio9 samples contained members of the Campylobacterota, Desulfobulbia and Zetaproteobacteria which were absent or in low abundance in samples of inactive

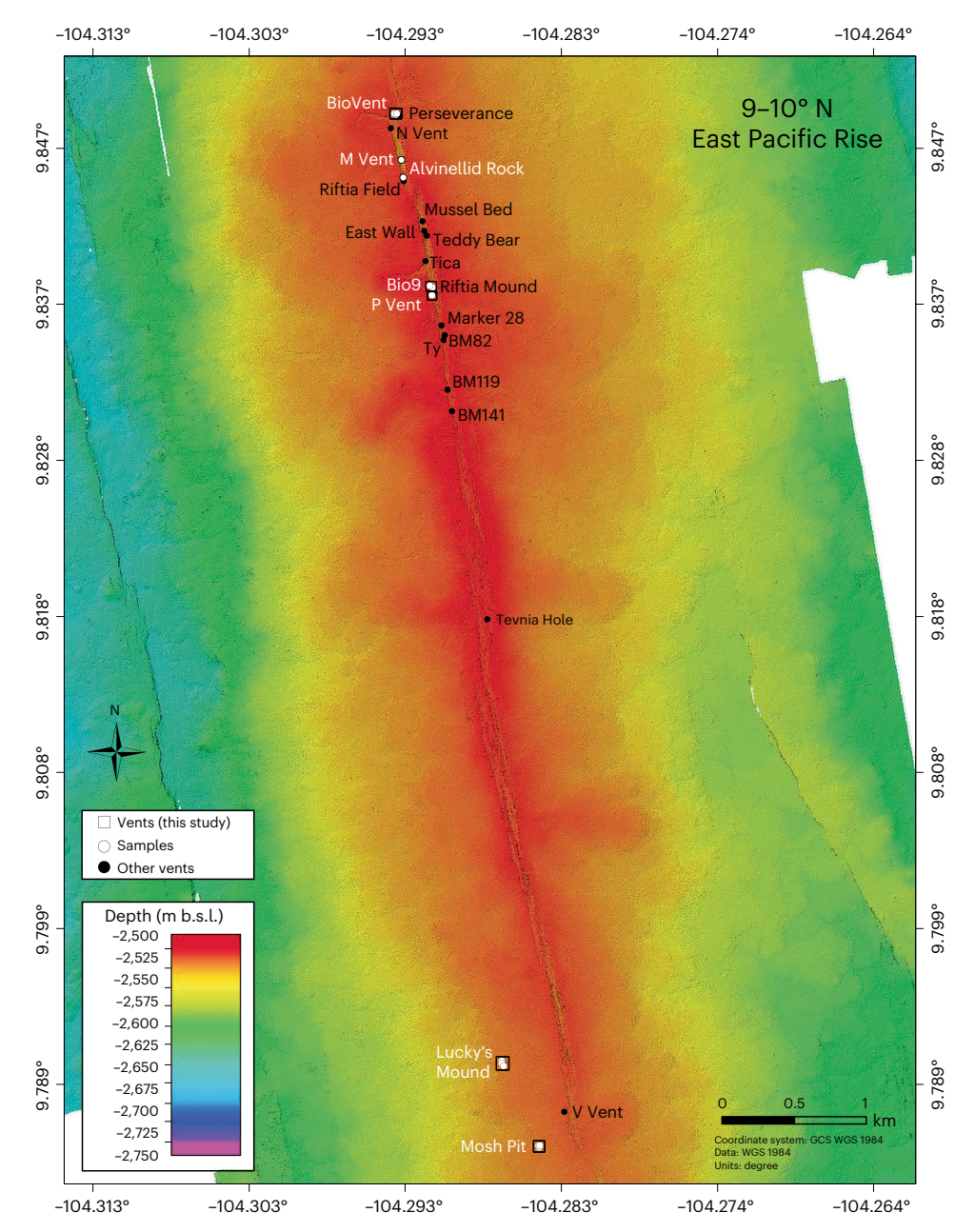


Fig. 1| **Bathymetry of the East Pacific Rise 9–10°** N **region.** Hydrothermal vents sampled in this study are outlined with black boxes and identified with white text. The locations of individual chimney deposits sampled are further denoted

with white circles. Black circles indicate the location of other hydrothermal vent chimneys in the region. m.b.s.l., meters below sea level; GCS, Geographic Coordinate System; WGS, World Geodetic System. Data from Wu et al. ⁵⁶.

deposits. Alternatively, taxa belonging to Acidimicrobiia, Nitrospiria, Thermodesulfovibrionia and Planctomycetia were present in samples from Mosh Pit and Lucky's Mound but rare in samples from Bio9 (Fig. 4a). The presence of Zetaproteobacteria is supported by scanning electron microscopy images of twisted stalks associated with this class (Fig. 4b)²⁷.

Marker genes for potential catabolism paired to carbon fixation were examined (Extended Data Fig. 5 and Supplementary Table 1). The dominant potential electron donors at all sites were inferred from this genomic data to be sulfur compounds followed by hydrogen, nitrogen and iron compounds. Dissimilatory pathways for both aerobic oxidation and anaerobic reduction pathways were detected on the same samples.

Genes involved in microbial inorganic carbon (Extended Data Table 2) fixation via the CBB cycle were most prevalent across all

inactive hydrothermal deposit samples followed by genes involved in the rTCA and WL pathway (Fig. 5a). Genes related to other pathways for inorganic carbon fixation were rare or absent from the samples examined.

Across all sites, CBB cycle genes were predominantly affiliated with members of the Alphaproteobacteria and Gammaproteobacteria (Fig. 5b and Supplementary Table 2). These genes were also associated with members of the Acidimicrobiia on inactive deposits from Lucky's Mound and Mosh Pit but were rare at the inactive-but-proximal site of Bio9. The genes for the CBB cycle were also detected in metagenome-assembled genomes (MAGs) of Rhodospirillales and UBA6615 families (Alphaproteobacteria) and Mariprofundales (Zetaproteobacteria). Among the rTCA cycle genes detected at Bio9, the majority were taxonomically related to members of the Campylobacteria (Supplementary Table 2). Conversely, at Mosh Pit, no

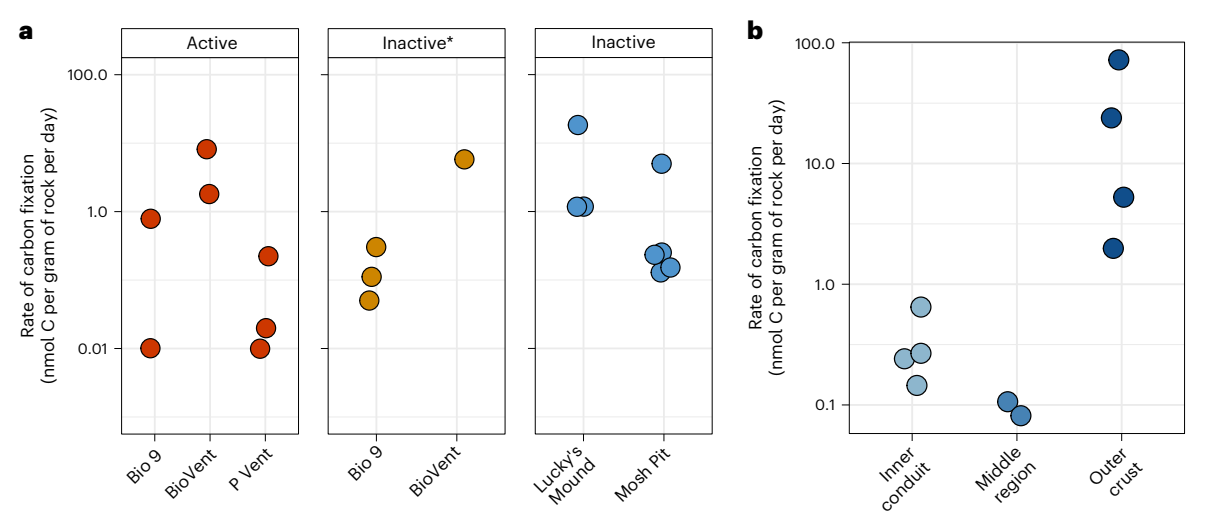


Fig. 2 | Assimilation of 14 C-bicarbonate by hydrothermal vent deposit hosted microbial communities. a, Rates of carbon fixation measured on bulk mineral deposits collected from active (n = 7; biologically independent samples), inactive-but-proximal (denoted as inactive*; n = 4) and inactive (n = 8) vents.

b, Carbon fixation rates measured from four subdivided samples collected from inactive vent deposits from Lucky's Mound (n=3) and Mosh Pit (n=1). Circles are averages of two to three replicate measurements.

Table 1 | Summary of carbon fixation rates on active, inactive-but-proximal and inactive hydrothermal vent deposits measured in this study

Average	Lower bound	Upper bound	Unit		
Inactive vent de	posits				
3.32	0.13	18.34	nmolCg ⁻¹ d ⁻¹		
14.55	0.58	80.23	μgCg ⁻¹ yr ⁻¹		
Inactive-but-pro	ximal vent deposit				
1.55	0.05	5.75	nmolCg ⁻¹ d ⁻¹		
6.81	0.21	25.21	μgCg ⁻¹ yr ⁻¹		
Active vent depo	osits				
1.38	0.01	8.17	nmolCg ⁻¹ d ⁻¹		
6.03	0.05	35.84	μgCg ⁻¹ yr ⁻¹		
Global estimate of primary productivity ^a					
8.73×10 ⁹	3.51×10 ⁸	4.82×10 ¹⁰	gCyr ⁻¹		

Rates are expressed as both nmol $Cg^{-1}d^{-1}$ and $\mu g Cg^{-1}yr^{-1}$ for ease of comparison. The values for inactive deposits were used to calculate an estimate of primary productivity on globally distributed inactive hydrothermal deposits. The global abundance of inactive hydrothermal deposits (°) is from Hannington et al.¹.

Campylobacteria were detected and rTCA genes instead belonged to Nitrospiria and UBA7883 (Nitrospinaceae) taxa (Supplementary Table 2). The rTCA genes detected at Lucky's Mound contained a mixture of these three lineages. These genes were further detected in MAGs classified as Sulfurimonas (Campylobacteria), JACRGQ01 (Nitrospinota), UBA8639 (Nitrospirota) and Desulfurobacteriales (Aquificota). Genes for the WL pathway typically showed greater phylogenetic diversity; however, many were associated with Desulfovibrionia and Thermodesulfovibrionia at Bio9 and Mosh Pit, respectively.

Stable isotope-based insight into microbial carbon fixation

The stable carbon isotope values of total organic carbon (TOC) were comparable for all chimney types. They range from -20.9% to -16.9% (average of 18.2%; Fig. 5c). In the inactive vent deposit from Mosh Pit, external versus inner material could be compared, revealing that the external material was 1% lighter. Polar lipid fatty acid (PLFA) derived

stable carbon isotope values were obtained for the main PLFAs: C16:0, C16:1, C18:0, C18:1 (Fig. 5c and Extended Data Table 3). The δ^{13} C of PLFAs from all hydrothermal vent deposit samples were on average approximately 7‰ lighter than the TOC values, ranging between -28.0% and -21.1% (average of 25.5‰).

Discussion

Inactive hydrothermal deposits are globally distributed and host ecosystems for which a scientific understanding is in its infancy. Currently, inactive deposits are being considered for seafloor mining due to their high concentrations of some base and precious metals, but research is lacking to inform management practices²⁵. In particular, data on ecosystem services are necessary to understand the role of inactive vent deposits in the deep-sea ecosystem²⁴. Primary productivity provides the base of a food web in any ecosystem and is therefore critical to quantify, especially before any significant anthropogenic disturbance such as that involved with most deep-sea mining techniques.

Previous work indicated the potential for microbial primary production on inactive hydrothermal deposits^{22,23,28,29}, but, to our knowledge, no studies have directly quantified carbon fixation rates. The study presented here provides definitive evidence for its presence in inactive vent systems. Incubation-based fixation rates of inorganic carbon measured in deposits collected from actively venting chimneys at EPR 9° 50′ N were comparable to rates for the inactive-but-proximal vent deposits, while inactive vent deposits were slightly higher, although not statistically different (Fig. 2a). Cell-normalized carbon fixation rates for active and inactive sulfides measured here were also similar and are comparable to rates in the deep ocean^{30,31}, surface sediments³² and diffuse hydrothermal fluids³³ (Supplementary Table 3). It should be noted that samples from active vents were incubated at 65 °C shipboard, lower than in situ temperatures, and in the absence of hydrothermal fluid. These incubation conditions may influence the natural microbiome response, and thus the rates measured for active vent deposits may be underestimations. Despite this, rates of primary production for deposits from both active and inactive vents measured in this study are comparable to those measured in samples previously collected from active vents on the Juan de Fuca Ridge³⁴ and East Pacific Rise³⁵, as well as vent fluids from the Mid-Atlantic Ridge³⁶, the Galapagos Spreading Center^{37,38} and East Pacific Rise³⁹, including experiments performed at in situ pressure (Extended Data Fig. 6).

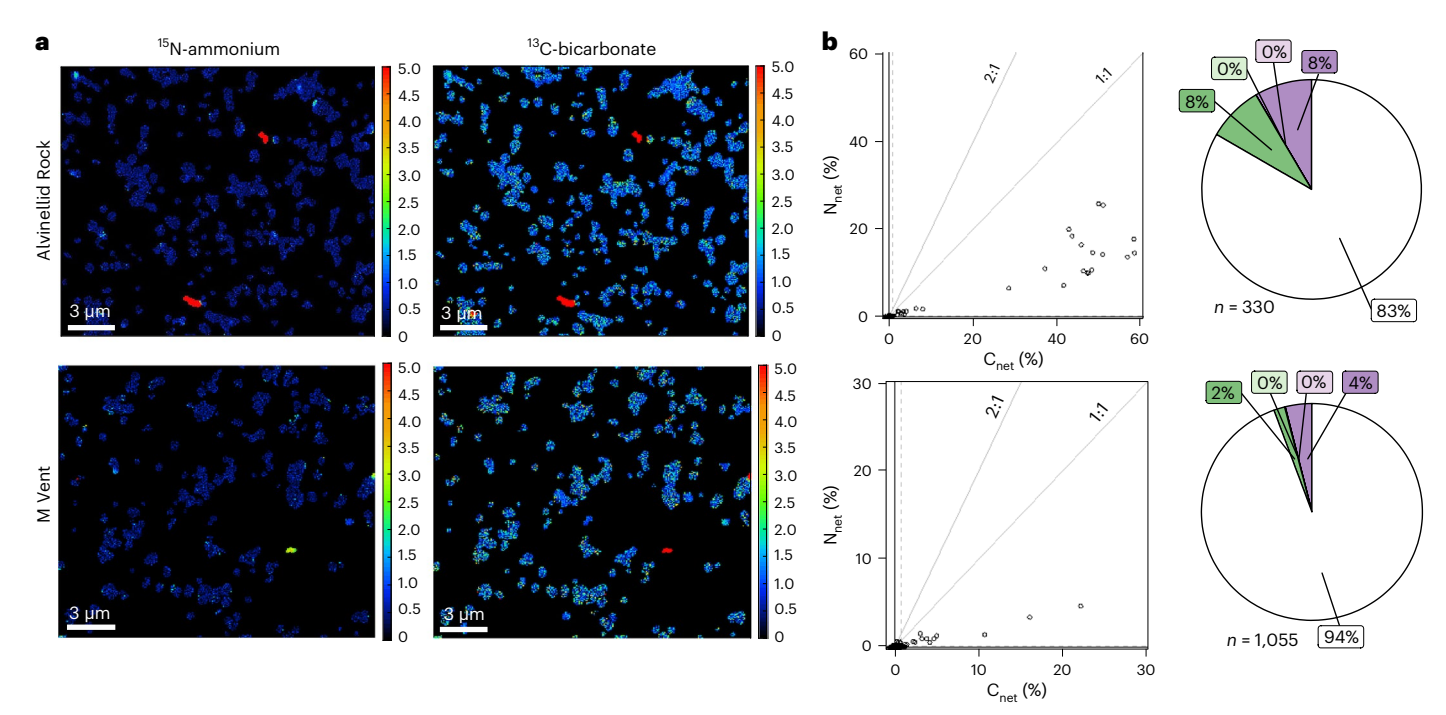


Fig. 3 | NanoSIMS analysis of ¹⁵N-ammonium and ¹³C-bicarbonate assimilation in individual microbial cells from active (Alvinellid Rock) and inactive (M Vent) hydrothermal vent deposits. **a**, Example fields of view from each site showing assimilation of ammonium (left) and bicarbonate (right) in two cells from Alvinellid Rock (top) and one from M Vent (bottom) after 7 days of incubation. Colour scale bars are in ¹⁵N or ¹³C atom %. **b**, Relative net assimilation of ammonium and bicarbonate in individual cells after 2 days of incubation from both Alvinellid Rock (top) and M Vent (bottom). Based on their relative assimilation of each substrate, the regions below the 2:1 line include

chemoautotrophic cells, the region above the 2:1 line includes heterotrophic cells, and the regions to the left (*x* axis) or below (*y* axis) the dashed lines includes cells below the detection limit of uptake for that substrate. Regions are defined as in Dekas et al.⁴¹ Data are summarized in the pie charts where chemoautotrophic cells are highlighted in green and heterotrophic cells are highlighted in purple with the total number of cells analysed indicated below each chart. Data are replotted in Extended Data Fig. 4 with truncated axes to better display data points around the origin (lower-activity cells and cells below the limit of detection).

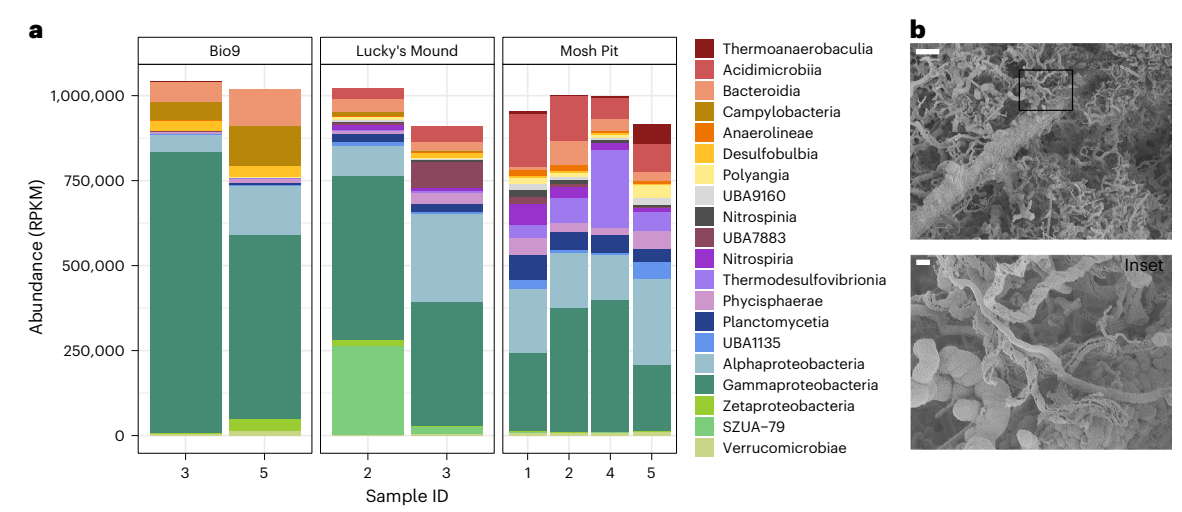


Fig. 4 | Microbial community composition from metagenomes on inactive (Lucky's Mound and Mosh Pit) and inactive-but-proximal (Bio9) hydrothermal vent deposits. a, Taxonomic distribution of GTDB annotated metagenomic reads shown at the class level. Normalized abundance is expressed as RPKM. Sample ID corresponds to those listed in Extended Data Table 1.

b, Representative scanning electron micrograph images showing examples of stalked features indicative of the presence of Zetaproteobacteria observed in surficial crustal rind on vent samples collected from Bio9. The lower image (scale bar, $1 \, \mu m$) is a magnification of the region in the upper image (scale bar, $10 \, \mu m$) outlined in black.

This comparison suggests that, despite the stated limitations, the rates measured in this study likely represent realistic primary production activity at the EPR and may also be reflective of rates for vent deposits found at other MOR, arc and back-arc systems.

The presence of autotrophically active microorganisms on hydrothermal vent deposits was further confirmed by the detection of incorporated ¹³C-bicarbonate into individual cells with nanoscale secondary ion mass spectrometry (nanoSIMS). Chemoautotrophs

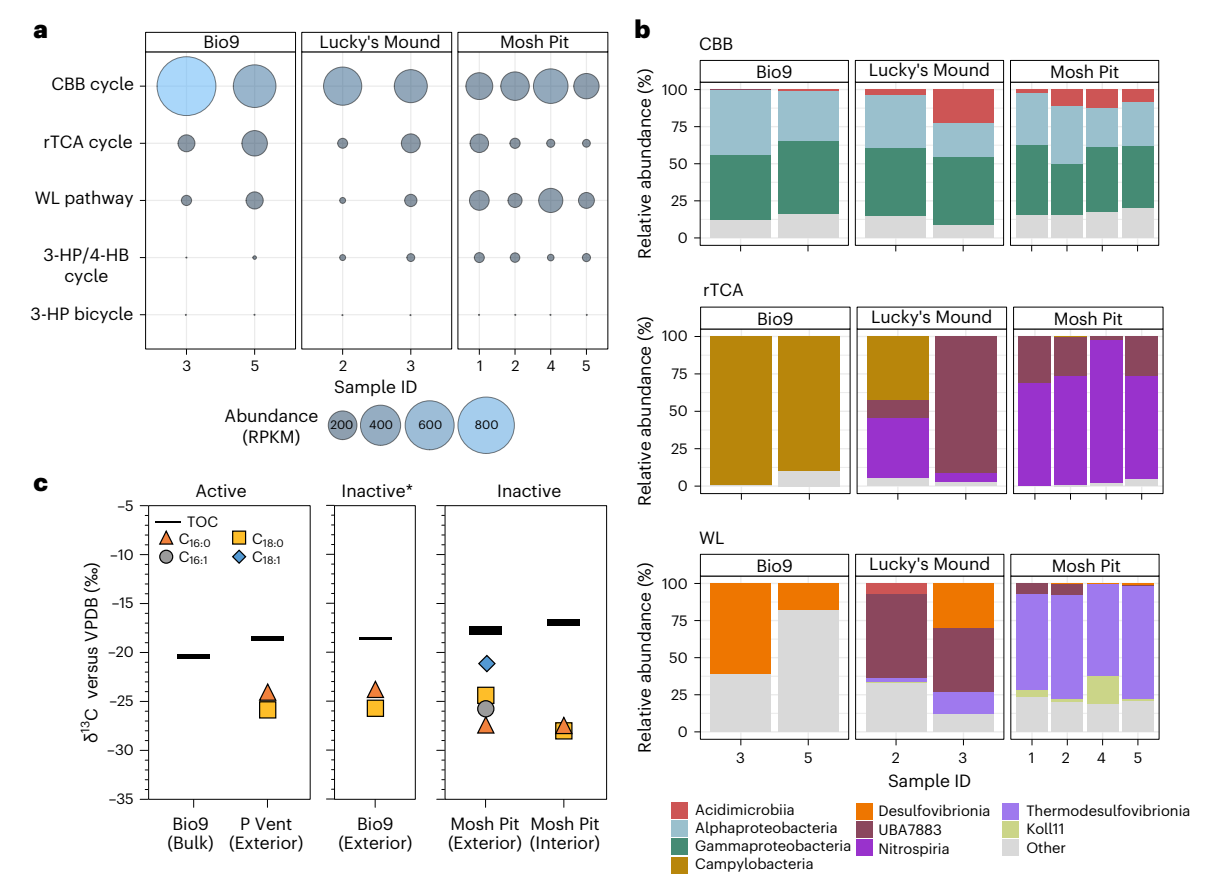


Fig. 5 | **Pathways of microbial carbon fixation on hydrothermal vent deposits. a**, The abundance of potential carbon fixation pathways on inactive (Lucky's Mound and Mosh Pit) and inactive-but-proximal (Bio9) hydrothermal vent deposits based on the presence of key genes for each metabolic pathway (Extended Data Table 2). Normalized abundance is expressed as RPKM. 3-HP, 3-hydroxypropionate; 4-HB, 4-hydroxybutryate. Sample ID corresponds to those listed in Extended Data Table 1. **b**, Taxonomic distribution of GTDB annotated

metagenomic reads for CBB, rTCA and WL pathways shown at the class level and expressed as the percentage relative abundance of total annotated reads for each metabolic pathway. **c**, Stable carbon isotopic composition (δ^{13} C) of TOC and the main PLFAs (C16:0, C18:0, C16:1, C18:1). For TOC all samples were measured in duplicates, except for the Bio9 exterior sample, which is a single measurement. VPDB. Vienna PeeDee Belemnite.

were found to make up a large fraction of the active microbial communities on active and inactive vent deposits. This assimilation was determined to reflect chemoautotrophy rather than inorganic carbon assimilation by heterotrophs (for example, via anaplerotic reactions) by comparing the ¹³C-uptake to the ¹⁵N-ammonium-uptake rates in each cell^{41,42}, with the latter being a proxy for total growth. Although higher mean assimilation was observed on the active vent deposit investigated by nanoSIMS compared to the inactive deposit (Extended Data Fig. 3), it is important to note that only one sample per vent type was analysed, and therefore, this comparison is not sufficient to draw broad conclusions about the difference between vent types.

Experiments examining the distribution of primary productivity along cross sections of individual inactive chimneys revealed that the outermost, Fe-oxyhydroxide-rich crust supported the highest rates of carbon fixation, followed by the inner central conduit and then the middle section (Fig. 2b and Extended Data Fig. 1b,c). A similar trend was observed for active chimneys by Wirsen et al. 36 , who found carbon fixation rates in surface scrapings of deposits were an order of magnitude higher than rates in internal material. In addition, the $\delta^{13}C_{\text{TOC}}$ values of external scraping from the outside wall of a sample from Mosh Pit were found to be lighter than that of the inner conduit material (Fig. 5c), further highlighting the small-scale intra-chimney heterogeneity of vent deposits. This supports previous findings that bacterial populations were also different between inner and outer

sections of inactive sulfides 14,19 . Such heterogeneity may be driven in part by redox gradients as well as colonization by seawater microorganisms. The large variance of primary production activity measured in samples collected over various spatial scales (<1 cm to >100 m; for example, Fig. 1) highlights the need to conduct such measurements with numerous samples to fully and accurately access the range of activity in global vent systems.

The microbial communities inhabiting inactive hydrothermal deposits across a range of sites at EPR 9° N are predicted to carry out carbon fixation via the CBB and rTCA cycles and the WL pathway (Fig. 5a). Carbon fixation via the rTCA cycle and WL pathway are generally found to be more prevalent in the higher temperature, microaerobic environments found at active hydrothermal vents 34,43-45, while the CBB cycle has been shown to typically dominate in inactive vents^{16,18,21,28}, as was observed in this study (Fig. 5a). The presence of both rTCA and CBB cycle utilizing microorganisms is further supported by an examination of the stable carbon isotope composition of TOC and lipids. These compounds have been previously used to evaluate the prevalent metabolisms in vent communities²¹, based on the observation that organisms utilizing the CBB cycle have large fractionation factors up to -30% or more compared to the inorganic carbon source, while the rTCA cycle fractionates the isotopes of carbon to a lesser degree^{46,47}. In our study the PLFAs point to CBB as the dominant carbon fixation pathway for the currently active bacterial community on inactive deposits (mean δ^{13} C = -25.5%; Fig. 5c). The δ^{13} C_{TOC} values are comparably heavy

(mean = −18.1‰), further hinting at the contribution of rTCA cycle utilizing microorganisms as well.

The average rate of primary productivity on the inactive hydrothermal deposits measured here in incubation-based experiments is sufficient to produce an amount of new organic carbon equivalent to ~10 5 cells per gram per day (assuming 94 fg of carbon per cell for cell volumes of 0.2 μm^3 as estimated by Khachikyan et al. 49). Based on protist grazing rates measured by Hu et al. 49 , this amount of organic carbon production would be sufficient to support protist populations on inactive vents of a similar magnitude to those found in hydrothermal vent fluids, providing an important link between chemosynthetic microbial communities and larger consumers within the food web including animal species documented on inactive deposits (reviewed in refs. 15,50,51).

Despite our growing understanding of the distribution, abundance and heterogeneity of active hydrothermal vent systems, our knowledge of inactive deposits is significantly lagging (for example, ref. 52). The discovery of inactive hydrothermal deposits is often by chance, but the recent implementation of high-resolution autonomous underwater vehicle (AUV)-based multibeam bathymetry surveys (~1 m gridded data) has expanded our ability to identify inactive deposits at variable distances from the MOR axis and our appreciation for the widespread extent of these features⁵³. Although we acknowledge the current inventory of inactive hydrothermal deposits is certainly an underestimation (for example, ref. 54) and recognize their physiochemical heterogeneity, it provides a valuable baseline to make an initial estimate of the importance of primary production on these features. If we extrapolate the primary productivity rates of inactive sulfide deposits measured via incubations in this study to the current best estimate for the global abundance of SMS deposits¹ as representative of potential substrate for microbial activity, we arrive at a carbon fixation rate of 3.51×10^8 to 4.82×10^{10} g C yr⁻¹ (Table 1). This maximum rate is comparable to estimates for global low temperature (5 °C) diffuse-flow systems estimated by McNichol et al. 40. Despite the caveats of these estimates, this work signifies that inactive deposits represent an important source of potential chemosynthetic productivity that has yet to be considered in evaluations of deep-sea biogeochemical carbon cycling.

The data presented here suggest that inactive hydrothermal deposits are important contributors to deep-sea carbon production. We show that rates of new organic carbon production in these inactive systems are comparable to rates on mineral deposits collected from actively venting hydrothermal chimneys. We further provide evidence that the chemoautotrophic members of the microbial community are highly active and likely predominately utilizing the CBB pathway. Although further work is required to understand how stable this new organic carbon production is over the lifetime of a deposit (from formation to potential burial under sediment or lava flows; for example, refs. 26,55,56) or how it varies with mineral composition, porosity and permeability, or host rock setting, the primary production shown here represents a vital ecosystem service provided by inactive deposits. This finding must be considered in regards to the current debate about seafloor mining^{24,25}. Such substantial and potentially devastating alteration of the seafloor demands a comprehensive assessment regarding this and other ecosystem services inactive deposits provide. This work provides an important step in that endeavour.

Methods

Site description and sample collection

The definition of active versus inactive vent is geologically and biologically important¹². Herein, samples are defined as 'active' if they were recovered from a structure that was actively venting visible hydrothermal fluid. 'Inactive' samples were collected from either hydrothermal talus (collapsed chimneys) or still upright but no longer venting chimneys. We further expand the terminology to include

'inactive-but-proximal' (also denoted as 'inactive*' in figures) to consider the impact of local hydrothermal venting on the biology and mineralogy of inactive vents located within tens of meters of active venting (Extended Data Table 1).

Samples were collected from active and inactive vent chimneys at East Pacific Rise crest 9° 50′ N (Fig. 1 and Extended Data Table 4) during three field expeditions: by Human Occupied Vehicle (HOV) Alvin during dives 5013, 5015, 5017 and 5019 in April 2019 on the AT42-09 cruise and during dives 5044-5046 in December 2019 on the AT42-21 cruise, both on RV Atlantis, and by Remotely Operated Vehicle (ROV) Jason during dive I2-1310 in April 2021 on the RR2102 cruise on the RV Roger Revelle. The manipulator arm of either HOV Alvin or ROV Jason was used to grab vent samples and place them in a sealable bio box on the vehicle's basket made of 1-inch thick high-density polyethylene plastic. The bio box was then closed for the duration of the dive. A Permatex gasket on the lid prevented surrounding seawater from entering the bio box during the dive and vehicle ascent. Before collection, the temperature of venting fluids was measured with the temperature probe (resolution ± 0.1 °C) on HOV Alvin for actively venting sulfides. Inactive hydrothermal deposits were probed in multiple places to determine temperatures were ambient and ensure that they were not venting.

Upon vehicle recovery at the end of a dive, water from the bio box was transferred to a pre-rinsed bucket. Three rinses of bio box water were swirled in the bucket and dumped before filling the bucket and then placing the sulfide sample in it. The sample was then taken to the lab and placed in a flame-sterilized steel rock box specifically designed for the sampling of seafloor rocks¹⁴. Subsamples of vent deposits were collected using a hammer and flame-sterilized chisel and placed into the appropriate storage containers depending on planned analyses.

Minerology

For each sample, polished 30 μ m thin sections were prepared for petrographic analysis of sample mineralogy under both transmitted and reflected light (for example, Extended Data Fig. 1a). This analysis included visually estimated mineral modal abundances and distributions, mineral paragenesis, and visual porosity estimates. Thin sections were cut perpendicular to chimney walls to expose a cross-section from the inner fluid conduit to the exterior of the sample.

Scanning electron microscopy

Biofilm from chimney deposits recovered from Bio9 were collected for scanning electron microscopy. External scrapings of the sample rock were preserved in 100% ethanol and stored under nitrogen. For analysis, the sample was subjected to critical-point drying then carbon coated using an ACE600 Sputter Coater before being imaged on a JEOL JSM-6500F scanning electron microscope (Characterization Facility, University of Minnesota-Twin Cities).

Cell enumeration

Shipboard preservation of hydrothermal vent chimney deposit samples for total cell enumeration was done by homogenizing subsamples in an acid-washed and flame-sterilized mortar and pestle. The sample was then mixed with five volumes of formalin (10%) and stored at 4 °C. Slides were prepared as described previously 57. Briefly, a 1 ml aliquot of the sample slurry was combined with 2.2 ml of 2.5% (w/v) NaCl, 0.4 ml methanol and 0.4 ml detergent solution (100 mM EDTA, 100 mM sodium pyrophosphate, 1%v/v Tween-80). Tubes were shaken at 500 rpm for 10 min using a Troemner Digital Multi-Tube Vortex Mixer before centrifugation at $3,000 \times g$ for 10 min. The resulting 1–1.5 ml of supernatant was stained with DAPI (final concentration 45 μ M) for 5 min in the dark before being filtered onto 25 mm, 0.2 μ m black polycarbonate filters and mounted onto glass slides. Ten fields of view were counted for each slide using an epifluorescence microscope (Zeiss Axio Imager M2) at ×1,000 magnification.

Bulk carbon fixation activity assays

Whole and subdivided (for example, Extended Data Fig. 1b) samples of hydrothermal vent chimney deposits (Extended Data Table 1) were used to establish shipboard incubations to quantify rates of inorganic carbon fixation. Incubations were started within 7 h of sample recovery at the surface. Samples were homogenized in an acid-washed and flame-sterilized mortar and pestle then mixed with an equal volume of 0.2 µm filter-sterilized bottom seawater collected by HOV Alvin in Niskin bottles away from hydrothermal venting activity. The homogenized slurry was then added in 1 ml aliquots to 8 ml glass vials containing an additional 4 ml of filter-sterilized bottom seawater (5 ml total volume). Three 1 ml aliquots of the sample slurry were also collected in 2 ml snap cap microcentrifuge tubes to estimate the average weight of vent material in the reaction vials. To each reaction vial, 1.5 uCi of ¹⁴C-sodium bicarbonate was added. Killed controls were terminated immediately after radiolabel addition by the addition of formaldehyde at 2% final concentration. Experimental samples were run in either duplicate or triplicate and incubated for 84 h. Hydrothermal deposits collected from actively venting chimney structures were incubated at 65 °C, while samples collected from inactive and inactive-but-proximal chimney structures were incubated near ambient at 4 °C.

Following incubation, the experimental samples were terminated with the addition of formaldehyde at 2% final concentration. Samples were immediately transferred to 5 ml centrifuge tubes and centrifuged at $500 \times g$ for 10 min to separate the mineral fraction from the aqueous solution. The supernatant was discarded, and the sulfide minerals were then washed twice with 2 ml of ultrapure (18.2 m Ω) water before being resuspended with a final 2 ml of water. The samples were acidified to pH < 4 by the addition of HCl and allowed to degas overnight with periodic mixing by shaking. The minerals were again collected by centrifugation, suspended in 2 ml filtered water and acidified a second time to pH < 4 by the addition of HCl. After degassing for 8–12 h, the samples were washed twice as described above and allowed to dry overnight. Once dry, the samples were mixed with 1 ml ultrapure water and 10 ml CytoScint-ES liquid scintillation cocktail (MP Biomedicals). The samples were then run on either a Hidex 300SL (Hidex) for incubations from cruise AT42-09 or a Tri-Carb 2910TR (PerkinElmer) liquid scintillation counter for incubations from cruise AT42-21 alongside ¹⁴C standards and counted for 20 min. Any radioactivity measured in the killed controls was subtracted from that measured in the respective experimental samples.

Rates of inorganic carbon fixation activity were calculated as described by Molari et al. 58 . Dissolved inorganic carbon concentrations were not directly measured at this site during the time of sample collection; therefore, dissolved inorganic carbon concentrations in bottom seawater from the 9° 50′ N region of the East Pacific Rise were taken from McNichol et al. 59 (for example, 2.3 mmol kg $^{-1}$). A two-tailed, unpaired Student's t-test was used to evaluate the significance (P< 0.05) of fixation rates between samples and vent types.

Single-cell carbon fixation assays and nanoSIMS analysis

Approximately $10~cm^3$ of hydrothermal vent deposits were placed into glass bottles containing ~50 ml of 0.2 μm filtered bottom seawater and amended with ^{15}N -ammonium and ^{13}C -bicarbonate to a final concentration of $5~\mu M$ and $1,000~\mu M$, respectively. The inactive chimney sample (M Vent) was incubated at $4~^{\circ}C$, while the active chimney sample (Alvinellid Rock) was incubated at $60~^{\circ}C$ (Fig. 1). All incubation bottles were wrapped with aluminium foil to maintain dark conditions. Active samples were incubated with completely sealed lids; inactive samples were incubated with loose lids to prevent anoxia. Samples for analysis were collected with no incubation (time point 0), after 2 days of incubation and after 7 days. Following incubation, several pieces of vent deposit were collected in 50 ml conical tubes and covered with 10% formalin. After 12-18~h at $4~^{\circ}C$, the formalin was removed from the tubes, and the samples were washed with phosphate-buffered saline (PBS).

After 5 min of incubation, the PBS was removed and finally replaced with a 50:50 mix of PBS:ethanol before freezing tubes at -20 °C. After returning to the laboratory, the vent samples were crushed, and fixed cells were separated from particles by ultrasonication and centrifugation. Cells were filtered onto 0.2 μ m gold-coated polycarbonate filters and frozen at -20 °C until nanoSIMS analysis.

Sections of filters were mounted onto adhesive dots and analysed with a CAMECA NanoSIMS 50 L housed in the Stanford Nano Facility at Stanford University. Analysis conditions were as described in Meyer et al. 60. The following masses were collected: 12C12C-, 12C13C- and 12C14N-, ¹²C¹⁵N⁻, ³²S⁻. Image analysis was performed in Look@NanoSIMS⁶¹, and nearly 5,000 carbon- and nitrogen-containing regions of interest (putative cells) were identified using the ³²S⁻ base image. Regions of interest with low ion count recovery (Poisson error greater than 0.1) were excluded. C_{net}% and N_{net}% were calculated as in Parada et al.⁶². The isotope fraction of the isotope label at the start of the incubation was determined using isotope mass balance of the quantity and isotope composition of the added substrate and that of the in situ pool of ammonium and bicarbonate. The in situ pool of ammonium was determined to be negligible (<10 nM) using a fluorometric quantification⁶³. The in situ pool of bicarbonate was assumed to be that of typical seawater (2.06 mM) and at natural abundance isotope values⁶⁴. Thresholds for active assimilation (relative to time point 0 values) and autotrophy versus heterotrophy (dependent on a cell's C_{net}% to N_{net}% ratio) were used as defined in Dekas et al. 41.

DNA extraction, metagenome sequencing and analysis

Inactive hydrothermal vent samples were primarily collected from Bio9, Mosh Pit and Lucky's Mound (Fig. 1). Representative samples were chosen from each of these sites for metagenomic analysis. For DNA extraction, approximately 5 g of sample was crushed with an autoclaved mortar and pestle and divided equally among five 2 ml screw-cap tubes containing 0.5 g sterile borosilicate glass beads (Biospec Products). To each tube, 700 µl of extraction buffer (100 mM Tris-HCl, 100 mM EDTA, 100 mM sodium phosphate, 1.5 M NaCl, 2% CTAB, pH 8) was added, and the sample was mixed on a vortex mixer for 5 min before bead beating for 30 s. Following mechanical lysis, 70 µl of 20% SDS was added, and the samples were incubated at 60 °C with shaking for 1 h. The samples were then centrifuged at $5,000 \times g$ for 10 min, and the supernatant was transferred to a 15 ml tube. The remaining solids were then processed a second time as described above. The supernatant resulting from the second round of extraction was pooled with the first, and an equal volume of phenol:chloroform:isoamyl alcohol solution was added. The samples were mixed well and centrifuged at $5,000 \times g$ for 10 min. The aqueous phase was transferred to a new 15 ml tube, and an equal volume of chloroform was added followed by mixing and centrifugation. The final aqueous phase was transferred to a new 2 ml tube, and the DNA was precipitated overnight at 4 °C with 0.6 volumes of 100% isopropanol and 0.3 M sodium acetate (pH 5.2, final concentration).

Extracted DNA was prepared for sequencing with the NEXFLEX rapid XP DNA-Seq HT library prep kit and run on a NovaSeq 6000 S4 at Texas A&M University AgriLife Genomics and Bioinformatics facility to generate 150 bp paired end reads. Raw metagenomic sequence reads were trimmed using Trimmomatic (v0.39)⁶⁵ to remove adaptors and low-quality base pairs (average quality = 30, minimum length = 75). All samples were then pooled and assembled with Megahit (v1.2.9)⁶⁶ using default parameters. Gene open reading frames were predicted with Prodigal (v2.6.3)⁶⁷, and individual sequence reads from each sample were then mapped to the genes using Bowtie2 (v2.5.0; sensitive flag)⁶⁸ to determine coverage across samples. The abundance of genes across samples was then calculated by expressing the number of mapped reads as reads per kilobase million (RPKM) values. Genes were taxonomically assigned based on comparison to the Genome Taxonomy Database (GTDB) (v207) using MMSeqs2 (default parameters)⁶⁹ and functionally assigned based on the Kyoto Encyclopedia of Genes and

Genomes ontology database with GhostKoala (v2.0)⁷⁰. Genes assigned to select enzymes for various carbon fixation pathways were specifically identified (Extended Data Table 2) in the entire metagenomic dataset as well as in MAGs (Supplementary Table 2). In addition, key genes involved in the potential use of oxygen, hydrogen, sulfur, nitrogen and iron species as redox couples were annotated based on hidden Markov models (HMMs) using MagicLamp (version unspecified)^{71,72} (Supplementary Table 1).

Stable carbon isotope ananlysis of TOC and PLFA

Hydrothermal vent deposits for stable carbon isotope analysis were collected from inactive (Mosh Pit), inactive-but-proximal (Bio9) and active (Bio9 and P Vent) chimneys (Fig. 1) using metal spatulas cleaned with methanol and dichloromethane. Subsamples were placed in combusted glass vials and then frozen until analysis onshore. For $\delta^{13}C_{TOC}$ analyses, 1 to 6 g of freeze-dried chimney material was homogenized with a solvent-cleaned mortar and pestle. Several milligrams of this sample material was analysed on a Thermo Scientific Flash 2000 elemental analyser connected to a Thermo Delta V Plus IRMS (Thermo Fisher Scientific) after decalcification with 10% HCl. The Isodat Gas Isotope Ratio MS software (v3.0.94.12, Thermo Fisher Scientific) was used for data processing. Isotopic values are reported in the delta notation as δ^{13} C (%) relative to the Vienna PeeDee Belemnite standard. The 1σ precision of repeated isotopic analysis (n = 4) of a lab standard from the sediments of the White Oak River estuary was below 0.1‰. Where possible, samples were analysed in duplicates.

For lipid analyses the remaining freeze-dried and homogenized chimney material was extracted using a modified Bligh and Dyer extraction technique after Sturt et al. 73. In short, a solvent mixture (v:v) of methanol (MeOH), dichloromethane (DCM) and aqueous buffer (2:1:0.8) was added to the samples and ultrasonicated for 10 min, and the supernatants were combined in a separatory funnel after centrifugation. In total, four steps of extraction were applied, twice with a phosphate buffer (8.7 g L⁻¹ KH₂PO₄, pH 7.4) and twice with a trichloroacetic acid buffer (50 g L⁻¹, pH 2). A fifth extraction step was added using only DCM:MeOH, 1:3 (v/v). In the separatory funnel, DCM and deionized water (MilliQ) were added for phase separation, and the combined extracts were washed subsequently three times with DCM and water. The organic phase was collected and dried under a gentle stream of nitrogen and stored at -20 °C. One gram of combusted sand was added to each sample to facilitate extraction. Separation of intact PLFAs from free fatty acids occurred after Meador et al. 4 using preparative normal-phase liquid chromatography-mass spectrometry with an Agilent 1200 series high-performance liquid chromatography coupled to an Agilent 1200 series Single Quad MS via an electrospray ionization interface. Compounds were separated on a Diol Inertsil column (5 μm, 10×150 mm) with a flow rate of 3 ml min⁻¹ and the following gradient: 100% A (n-hexane:2-propanol, 85:15, v/v) to 10% B (isopropanol: H_2O , 9:1, v/v) in 5 min, to 85% B in 1 min, hold for 9 min; the column was re-equilibrated with 100% A for 6 min before the next injection. The apolar (free fatty acid containing) fraction was collected in the first 5 min, the polar (PLFA containing) fraction from 5 to 15 min. Aliquots of sample fractions were reanalysed on high-performance liquid chromatography-quadrupole-time-of-flight-mass spectrometry (Bruker) to check the separation and purity of the fractions⁷⁵. For this the software Bruker Compass Data Analysis (v4.4, Bruker Daltonics) was used.

The polar fraction was subsequently acid hydrolysed using 5% HCl in methanol at $70\,^{\circ}$ C for 1 h and subjected to silica column chromatography to yield fatty acid methyl esters. The polar lipid-derived fatty acid methyl ester was analysed on an Agilent 7890A-GC, interfaced to an Agilent 5975C VL MSD for compound identification using Thermo Scientific XCalibur (v 4.1.50, Thermo Fisher Scientific) and a Thermo Scientific Trace GC isolink coupled to a Delta V Plus IRMS via GC IsoLink connected to a ConFlow IV interface (Thermo Fisher Scientific) to obtain compound-specific isotope values using the Isodat Gas Isotope

Ratio MS software (v3.0.94.12, Thermo Fisher Scientific). Compounds were separated on Restek Rxi-5 ms column (30 m length; 0.25 mm i.d.; 0.25 µm film thickness, Restek) using helium as carrier gas at a constant flow rate of 1 ml min $^{-1}$. Split less injection was performed at 300–310 °C. The 1σ precision of duplicate isotopic analysis of a fatty acid standard mixture was \leq 0.5‰. The reported δ^{13} C values were corrected for the introduction of additional carbon atoms during acid hydrolysis with methanol.

Reporting summary

Further information on research design is available in the Nature Portfolio Reporting Summary linked to this article.

Data availability

Raw metagenomic data are available in the NCBI Sequence Read Archive (SRA) under BioProject PRJNA998752.

References

- Hannington, M., Jamieson, J., Monecke, T., Petersen, S. & Beaulieu, S. The abundance of seafloor massive sulfide deposits. Geology 39, 1155–1158 (2011).
- Haymon, R. M. Growth history of hydrothermal black smoker chimneys. Nature 301, 695–698 (1983).
- 3. Van Dover, C. L. in *The Ecology of Deep-Sea Hydrothermal Vents* (Princeton Univ. Press, 2021).
- Jannasch, H. W. & Wirsen, C. O. Chemosynthetic primary production at East Pacific sea floor spreading centers. *Bioscience* 29, 592–598 (1979).
- Corliss, J. B. et al. Submarine thermal springs on the Galapagos Rift. Science 203, 1073–1083 (1979).
- Jamieson, J. W. et al. Sulfide geochronology along the Endeavour Segment of the Juan de Fuca Ridge. Geochem. Geophys. Geosyst. 14, 2084–2099 (2013).
- Cherkashov, G. et al. Sulfide geochronology along the northern equatorial Mid-Atlantic Ridge. Ore Geol. Rev. 87, 147–154 (2017).
- 8. Jamieson, J. W., Galley, C., McNeil, N. & Mora, D. S. Evaluating episodicity of high-temperature venting within seafloor hydrothermal vent fields. *Earth Planet. Sci. Lett.* **606**, 118051 (2023).
- Lalou, C., Reyss, J. L. & Brichet, E. Age of sub-bottom sulfide samples at the TAG active mound. In *Proc. Ocean Drilling Program* 158 (Texas A&M University, 1998).
- Kuznetsov, V. et al. The oldest seafloor massive sulfide deposits at the Mid-Atlantic Ridge: Th/U chronology and composition. Geochronometria 42, 100–106 (2015).
- 11. Kuznetsov, V. et al. ²³⁰Th/U chronology of ore formation within the Semyenov hydrothermal district (13° 31′ N) at the Mid-Atlantic ridge. *Geochronometria* **38**, 72–76 (2011).
- Jamieson, J. W. & Gartman, A. Defining active, inactive, and extinct seafloor massive sulfide deposits. *Mar. Policy* 117, 103926 (2020).
- Petersen, S. et al. News from the seabed—geological characteristics and resource potential of deep-sea mineral resources. Mar. Policy 70, 175–187 (2016).
- Sylvan, J. B., Toner, B. M. & Edwards, K. J. Life and death of deep-sea vents: bacterial diversity and ecosystem succession on inactive hydrothermal sulfides. MBio 3, e00279–00211 (2012).
- Van Dover, C. L. Inactive sulfide ecosystems in the deep sea: a review. Front. Mar. Sci. 6, 461 (2019).
- Hou, J. et al. Microbial succession during the transition from active to inactive stages of deep-sea hydrothermal vent sulfide chimneys. *Microbiome* 8, 1–18 (2020).
- Kato, S. et al. Biogeography and biodiversity in sulfide structures of active and inactive vents at deep-sea hydrothermal fields of the Southern Mariana Trough. Appl. Environ. Microbiol. 76, 2968–2979 (2010).

- Kato, S. et al. Potential for biogeochemical cycling of sulfur, iron and carbon within massive sulfide deposits below the seafloor. *Environ. Microbiol.* 17, 1817–1835 (2015).
- 19. Sylvan, J. B. et al. Low temperature geomicrobiology follows host rock composition along a geochemical gradient in Lau Basin. *Front. Microbiol.* **4**, 61 (2013).
- 20. Toner, B. M. et al. Mineralogy drives bacterial biogeography of hydrothermally inactive seafloor sulfide deposits. *Geomicrobiol. J.* **30**, 313–326 (2013).
- Reeves, E. P. et al. Microbial lipids reveal carbon assimilation patterns on hydrothermal sulfide chimneys. *Environ. Microbiol.* 16, 3515–3532 (2014).
- Meier, D. V. et al. Microbial metal-sulfide oxidation in inactive hydrothermal vent chimneys suggested by metagenomic and metaproteomic analyses. *Environ. Microbiol.* 21, 682–701 (2019).
- Dong, X. et al. Functional diversity of microbial communities in inactive seafloor sulfide deposits. FEMS Microbiol. Ecol. 97, fiab108 (2021).
- Orcutt, B. N. et al. Impacts of deep-sea mining on microbial ecosystem services. Limnol. Oceanogr. 65, 1489–1510 (2020).
- Van Dover, C. L. et al. Research is needed to inform environmental management of hydrothermally inactive and extinct polymetallic sulfide (PMS) deposits. *Mar. Policy* 121, 104183 (2020).
- Fornari, D. J. et al. The East Pacific Rise between 9 N and 10 N: twenty-five years of integrated, multidisciplinary oceanic spreading center studies. Oceanography 25, 18–43 (2012).
- 27. McAllister, S. M. et al. The Fe (II)-oxidizing Zetaproteobacteria: historical, ecological and genomic perspectives. *FEMS Microbiol. Ecol.* **95**, fiz015 (2019).
- Kato, S. et al. Genome-enabled metabolic reconstruction of dominant chemosynthetic colonizers in deep-sea massive sulfide deposits. *Environ. Microbiol.* 20, 862–877 (2018).
- Pan, J. et al. Genome-resolved evidence for functionally redundant communities and novel nitrogen fixers in the deyin-1 hydrothermal field, Mid-Atlantic Ridge. *Microbiome* 10, 1–20 (2022).
- Günter, J., Zubkov, M. V., Yakushev, E., Labrenz, M. & Jürgens, K. High abundance and dark CO₂ fixation of chemolithoautotrophic prokaryotes in anoxic waters of the Baltic Sea. *Limnol. Oceanogr.* 53, 14–22 (2008).
- Herndl, G. J. et al. Contribution of Archaea to total prokaryotic production in the deep Atlantic Ocean. Appl. Environ. Microbiol. 71, 2303–2309 (2005).
- Dyksma, S. et al. Ubiquitous Gammaproteobacteria dominate dark carbon fixation in coastal sediments. *ISME J.* 10, 1939–1953 (2016).
- McNichol, J. et al. Genus-specific carbon fixation activity measurements reveal distinct responses to oxygen among hydrothermal vent Campylobacteria. Appl. Environ. Microbiol. 88, e02083–02021 (2022).
- Olins, H., Rogers, D., Frank, K., Vidoudez, C. & Girguis, P. Assessing the influence of physical, geochemical and biological factors on anaerobic microbial primary productivity within hydrothermal vent chimneys. *Geobiology* 11, 279–293 (2013).
- Bonch-Osmolovskaya, E. A. et al. Activity and distribution of thermophilic prokaryotes in hydrothermal fluid, sulfidic structures, and sheaths of alvinellids (East Pacific Rise, 13 N). Appl. Environ. Microbiol. 77, 2803–2806 (2011).
- Wirsen, C. O., Jannasch, H. W. & Molyneaux, S. J. Chemosynthetic microbial activity at Mid-Atlantic Ridge hydrothermal vent sites. J. Geophys. Res. Solid Earth 98, 9693–9703 (1993).
- Tuttle, J., Wirsen, C. & Jannasch, H. Microbial activities in the emitted hydrothermal waters of the Galapagos Rift vents. *Mar. Biol.* 73, 293–299 (1983).

- Mandernack, K. W. & Tebo, B. M. In situ sulfide removal and CO₂ fixation rates at deep-sea hydrothermal vents and the oxic/anoxic interface in Framvaren Fjord, Norway. *Mar. Chem.* 66, 201–213 (1999).
- Wirsen, C. O., Tuttle, J. & Jannasch, H. Activities of sulfur-oxidizing bacteria at the 21 N East Pacific Rise vent site. *Mar. Biol.* 92, 449–456 (1986).
- McNichol, J. et al. Primary productivity below the seafloor at deep-sea hot springs. *Proc. Natl Acad. Sci. USA* 115, 6756–6761 (2018).
- Dekas, A. E. et al. Characterizing chemoautotrophy and heterotrophy in marine archaea and bacteria with single-cell multi-isotope NanoSIP. Front. Microbiol. 10, 2682 (2019).
- Braun, A. et al. Reviews and syntheses: heterotrophic fixation of inorganic carbon-significant but invisible flux in environmental carbon cycling. *Biogeosciences* 18, 3689–3700 (2021).
- Wang, F. et al. GeoChip-based analysis of metabolic diversity of microbial communities at the Juan de Fuca Ridge hydrothermal vent. Proc. Natl Acad. Sci. USA 106, 4840–4845 (2009).
- Hügler, M. & Sievert, S. M. Beyond the Calvin cycle: autotrophic carbon fixation in the ocean. *Annu. Rev. Mar. Sci.* 3, 261–289 (2011).
- 45. Sievert, S. M. & Vetriani, C. Chemoautotrophy at deep-sea vents: past, present, and future. *Oceanography* **25**, 218–233 (2012).
- House, C. H., Schopf, J. W. & Stetter, K. O. Carbon isotopic fractionation by Archaeans and other thermophilic prokaryotes. *Org. Geochem.* 34, 345–356 (2003).
- Havig, J. R., Raymond, J., Meyer-Dombard, D. A. R., Zolotova, N. & Shock, E. L. Merging isotopes and community genomics in a siliceous sinter-depositing hot spring. *J. Geophys. Res. Biogeosciences* 116, G01005 (2011).
- 48. Khachikyan, A. et al. Direct cell mass measurements expand the role of small microorganisms in nature. *Appl. Environ. Microbiol.* **85**, e00493–00419 (2019).
- Hu, S. K. et al. Protistan grazing impacts microbial communities and carbon cycling at deep-sea hydrothermal vents. *Proc. Natl Acad. Sci. USA* 118, e2102674118 (2021).
- Boschen, R. E., Rowden, A. A., Clark, M. R. & Gardner, J. P. Mining of deep-sea seafloor massive sulfides: a review of the deposits, their benthic communities, impacts from mining, regulatory frameworks and management strategies. *Ocean Coast. Manag.* 84, 54–67 (2013).
- 51. Neufeld, M., Metaxas, A. & Jamieson, J. W. Non-vent megafaunal communities on the Endeavour and Middle Valley segments of the Juan de Fuca Ridge, Northeast Pacific Ocean. *Front. Mar. Sci.* **9**, 804 (2022).
- Beaulieu, S. & Szafranski, K. InterRidge Global Database of Active Submarine Hydrothermal Vent Fields Version 3.4. World Wide Web Electronic Publication (accessed 2020); http://vents-data. interridge.org
- 53. Minami, H. & Ohara, Y. The Gondou hydrothermal field in the Ryukyu Arc: a huge hydrothermal system on the flank of a caldera volcano. *Geochem. Geophys. Geosyst.* **18**, 3489–3516 (2017).
- 54. Jamieson, J., Clague, D. & Hannington, M. D. Hydrothermal sulfide accumulation along the Endeavour segment, Juan de Fuca Ridge. *Earth Planet*. Sci. Lett. **395**, 136–148 (2014).
- Fornari, D. J., Haymon, R. M., Perfit, M. R., Gregg, T. K. & Edwards, M. H. Axial summit trough of the East Pacific Rice 9°–10° N: geological characteristics and evolution of the axial zone on fast spreading mid-ocean ridge. J. Geophys. Res. Solid Earth 103, 9827–9855 (1998).
- Wu, J. N. et al. Extent and volume of lava flows erupted at 9 50'N, East Pacific Rise in 2005–2006 from autonomous underwater vehicle surveys. Geochem. Geophys. Geosyst. 23, e2021GC010213 (2022).

- Monteverde, D. R. et al. Distribution of extracellular flavins in a coastal marine basin and their relationship to redox gradients and microbial community members. *Environ. Sci. Technol.* 52, 12265–12274 (2018).
- Molari, M., Manini, E. & Dell'Anno, A. Dark inorganic carbon fixation sustains the functioning of benthic deep-sea ecosystems. Glob. Biogeochem. Cycles 27, 212–221 (2013).
- McNichol, J. et al. Assessing microbial processes in deep-sea hydrothermal systems by incubation at in situ temperature and pressure. Deep Sea Res. I 115, 221–232 (2016).
- Meyer, N. R., Fortney, J. L. & Dekas, A. E. NanoSIMS sample preparation decreases isotope enrichment: magnitude, variability and implications for single-cell rates of microbial activity. *Environ. Microbiol.* 23, 81–98 (2021).
- 61. Polerecky, L. et al. Look@ NanoSIMS-a tool for the analysis of nanoSIMS data in environmental microbiology. *Environ. Microbiol.* **14**, 1009–1023 (2012).
- 62. Parada, A. E. et al. Constraining the composition and quantity of organic matter used by abundant marine Thaumarchaeota. *Environ. Microbiol.* **25**, 689–704 (2023).
- 63. Holmes, R. M., Aminot, A., Kérouel, R., Hooker, B. A. & Peterson, B. J. A simple and precise method for measuring ammonium in marine and freshwater ecosystems. *Can. J. Fish. Aquat. Sci.* **56**, 1801–1808 (1999).
- Rosman, K. & Taylor, P. Isotopic compositions of the elements 1997 (Technical Report). Pure Appl. Chem. 70, 217–235 (1998).
- 65. Bolger, A. M., Lohse, M. & Usadel, B. Trimmomatic: a flexible trimmer for Illumina sequence data. *Bioinformatics* **30**, 2114–2120 (2014).
- Li, D., Liu, C.-M., Luo, R., Sadakane, K. & Lam, T.-W. MEGAHIT: an ultra-fast single-node solution for large and complex metagenomics assembly via succinct de Bruijn graph. *Bioinformatics* 31, 1674–1676 (2015).
- Hyatt, D. et al. Prodigal: prokaryotic gene recognition and translation initiation site identification. *BMC Bioinform.* 11, 119 (2010).
- 68. Langmead, B. & Salzberg, S. L. Fast gapped-read alignment with Bowtie 2. *Nat. Methods* **9**, 357–359 (2012).
- Steinegger, M. & Söding, J. MMseqs2 enables sensitive protein sequence searching for the analysis of massive data sets.
 Nat. Biotechnol. 35, 1026–1028 (2017).
- Kanehisa, M., Sato, Y. & Morishima, K. BlastKOALA and GhostKOALA: KEGG tools for functional characterization of genome and metagenome sequences. J. Mol. Biol. 428, 726–731 (2016).
- Garber, A. I. et al. FeGenie: a comprehensive tool for the identification of iron genes and iron gene neighborhoods in genome and metagenome assemblies. Front. Microbiol. 11, 13 (2020).
- Garber, A., Ramirez, G. A., Merino, N., Pavia M. J., McAllister, S. M. MagicLamp: toolkit for annotation of genomic data using discreet and curated HMM sets. MagicLamp, GitHub repository (2023); https://github.com/Arkadiy-Garber/ MagicLamp
- 73. Sturt, H. F., Summons, R. E., Smith, K., Elvert, M. & Hinrichs, K. U. Intact polar membrane lipids in prokaryotes and sediments deciphered by high-performance liquid chromatography/ electrospray ionization multistage mass spectrometry—new biomarkers for biogeochemistry and microbial ecology. *Rapid Commun. Mass Spectrom.* 18, 617–628 (2004).
- Meador, T. B., Zhu, C., Elling, F. J., Könneke, M. & Hinrichs, K.-U. Identification of isoprenoid glycosidic glycerol dibiphytanol diethers and indications for their biosynthetic origin. Org. Geochem. 69, 70–75 (2014).

 Wörmer, L., Lipp, J. S., Schröder, J. M. & Hinrichs, K.-U. Application of two new LC–ESI–MS methods for improved detection of intact polar lipids (IPLs) in environmental samples. *Org. Geochem.* 59, 10–21 (2013).

Acknowledgements

We thank the captain and shipboard crew of the RV Atlantis during the AT42-09 and AT42-21 expeditions and of the RV Roger Revelle during the RR2102 expedition. We are also thankful for the input and hard work of the pilots and crew of the HOV Alvin, ROV Jason and AUV Sentry; the science done for this project would not be possible without the support of and collaboration with University-National Oceanographic Laboratory System operators and vessels and the National Deep Submergence Facility at Woods Hole Oceanographic Institution. This work was supported by grants from the US National Science Foundation to J.B.S. (OCE 1756339), B.M.T. (OCE 1756558), M.K.T. (OCE 1756419), D.J.F. (OCE 1949485) and A.E.D. (NSF CAREER award 2143035). J.B.S. acknowledges support from a Simons Foundation Early Career Investigator in Aquatic Microbial Ecology and Evolution Award. J.J. acknowledges financial support from the Canada Research Chairs program (CRC-2020-001165). S.M. acknowledges funding support from the Natural Sciences and Engineering Research Council of Canada Collaborative Research and Training Experience project in Marine Geodynamics and Georesources program. E.P.R. acknowledges funding support from the University of Bergen Meltzer Fund. We thank Emily Paris in the Dekas Laboratory for performing the ammonium quantification. The Stanford Nano Shared Facilities where the nanoSIMS analyses were conducted is supported in part by the National Science Foundation under award ECCS-2026822. F.S., J.B. and A.M. acknowledge funding from the German Research Foundation (DFG) under Germany's Excellence Strategy—EXC 2077-390741603. Finally, thank you to T. Meek (Texas A&M University) for providing access to liquid scintillation counting equipment.

Author contributions

J.B.S., B.M.T., M.K.T. and A.M.A. conceived the study. A.M.A., J.B.S., J.J., A.E.D. and F.S. wrote the manuscript with input from all authors. D.J.F. contributed site survey information and provided support for field work. A.M.A., R.J., C.P.H., E.P.R. and J.B. performed sample collection. A.M.A. performed carbon fixation measurements and conducted bioinformatic analysis. R.J. contributed scanning electron microscopy images. J.J. and S.M. performed mineralogical analysis. A.E.D. and N.R.M. performed NanoSIMS analysis. F.S. and A.M. performed analysis of TOC and PLFA. C.P.H. performed cell counts. All authors reviewed and approved the final manuscript.

Competing interests

The authors declare no competing interests.

Additional information

Extended data is available for this paper at https://doi.org/10.1038/s41564-024-01599-9.

Supplementary information The online version contains supplementary material available at https://doi.org/10.1038/s41564-024-01599-9.

Correspondence and requests for materials should be addressed to Amanda M. Achberger or Jason B. Sylvan.

Peer review information *Nature Microbiology* thanks the anonymous reviewers for their contribution to the peer review of this work.

Reprints and permissions information is available at www.nature.com/reprints.

Publisher's note Springer Nature remains neutral with regard to jurisdictional claims in published maps and institutional affiliations.

Springer Nature or its licensor (e.g. a society or other partner) holds exclusive rights to this article under a publishing agreement with the author(s) or other rightsholder(s); author

self-archiving of the accepted manuscript version of this article is solely governed by the terms of such publishing agreement and applicable law.

@ The Author(s), under exclusive licence to Springer Nature Limited 2024

Extended Data Table 1 | Summary list of samples used to measure carbon fixation assimilation rates (14C-bicarbonate) including mineralogical and biological characteristics

Sample ID (by location)	Dive	Activity	Sample Type	Dominant Mineralogy ^a	Porosity (%) ^a	Average Carbon fixation rates (nmol C g ⁻¹ d ⁻¹)	Cells g ⁻¹
P Vent 1	ALV5017	Active	Bulk			0.22	6.70E+05
P Vent 2						0.02	1.07E+09
P Vent 3						0.01	5.43E+08
Bio91	ALV5013	Active (Tmax 286°C)	Bulk	sp, po, anh, ccp, mc	40	0.78	1.78E+08
Bio92						0.01	4.57E+05
Bio9 3 ^b	ALV5015	Inactive*	Bulk	py, feooh, po, ccp, sp, anh, mc	20	0.05	1.47E+07
Bio9 4						0.11	1.38E+06
Bio9 5 ^b						0.3	1.17E+06
BioVent 1	ALV5046	Active (T _{max} 303°C)	Bulk	anh, py, feooh	50	1.79	1.50E+07
BioVent 2		Active (T _{max} 300°C)	Bulk	sp, py, mc, ccp	60	8.17	2.00E+08
BioVent 3		Inactive*	Bulk	sp, mc, ccp, py, feooh	20	5.75	4.50E+07
Mosh Pit 1 ^b	ALV5019	Inactive	Bulk	сср, ру	30	0.13	NA
Mosh Pit 2 ^b						0.25	7.94E+08
Mosh Pit O	ALV5019	Inactive	Bulk	ccp, feooh, py	35	NA	NA
Mosh Pit 3						0.23	2.13E+07
Mosh Pit 4 ^b						0.15	1.51E+08
Mosh Pit 5 ^b	ALV5044	Inactive	Bulk			5.08	NA
Mosh Pit 5A			Inner	mc, py, ccp, anh, sp, feooh	35	0.24	NA
Mosh Pit 5B			Middle	mc, py, ccp, anh, sp, feooh	35	0.11	NA
Mosh Pit 5C			Outer	feooh	35	24.52	NA
Lucky's Mound 1	ALV5044	Inactive	Bulk			1.19	NA
Lucky's Mound 1A			Inner	sp, ccp	30	0.15	NA
Lucky's Mound 1B			Middle	ccp, sp, py	20	0.08	NA
Lucky's Mound 1C			Outer	ccp, py, feooh, atac, sp	10	5.24	NA
Lucky's Mound 2 ^b	ALV5045	Inactive	Bulk			1.19	3.83E+07
Lucky's Mound 2A			Inner	py, feooh	25	0.66	NA
Lucky's Mound 2B			Outer	feooh, atac	25	1.92	NA
Lucky's Mound 3 ^b	ALV5045	Inactive	Bulk			18.34	8.88E+05
Lucky's Mound 3A			Inner	mc, ccp	5	0.27	NA
Lucky's Mound 3B			Outer	feooh	4	74.88	NA
	and the second			The second of the second	()	. (0 01/01/1)	. (0 = 0)

 a Visually estimated from thin section b Denotes samples used for metagenomics Mineral abbreviations: anh, anhydrite (CaSO₄); atac, atacamite (Cu₂Cl(OH)₃); ccp, chalcopyrite (CuFeS₂); Fe-oxyhydroxide (FeO(OH); mc, marcasite (FeS₂); py, pyrite (FeS₂); po, pyrrhotite (FeS₂); ps, sp, sphalerite (ZnS)

$\textbf{Extended Data Table 2} \ | \ \textbf{Key marker genes used to identify the presence of carbon fixation pathways in metagenomic datasets}$

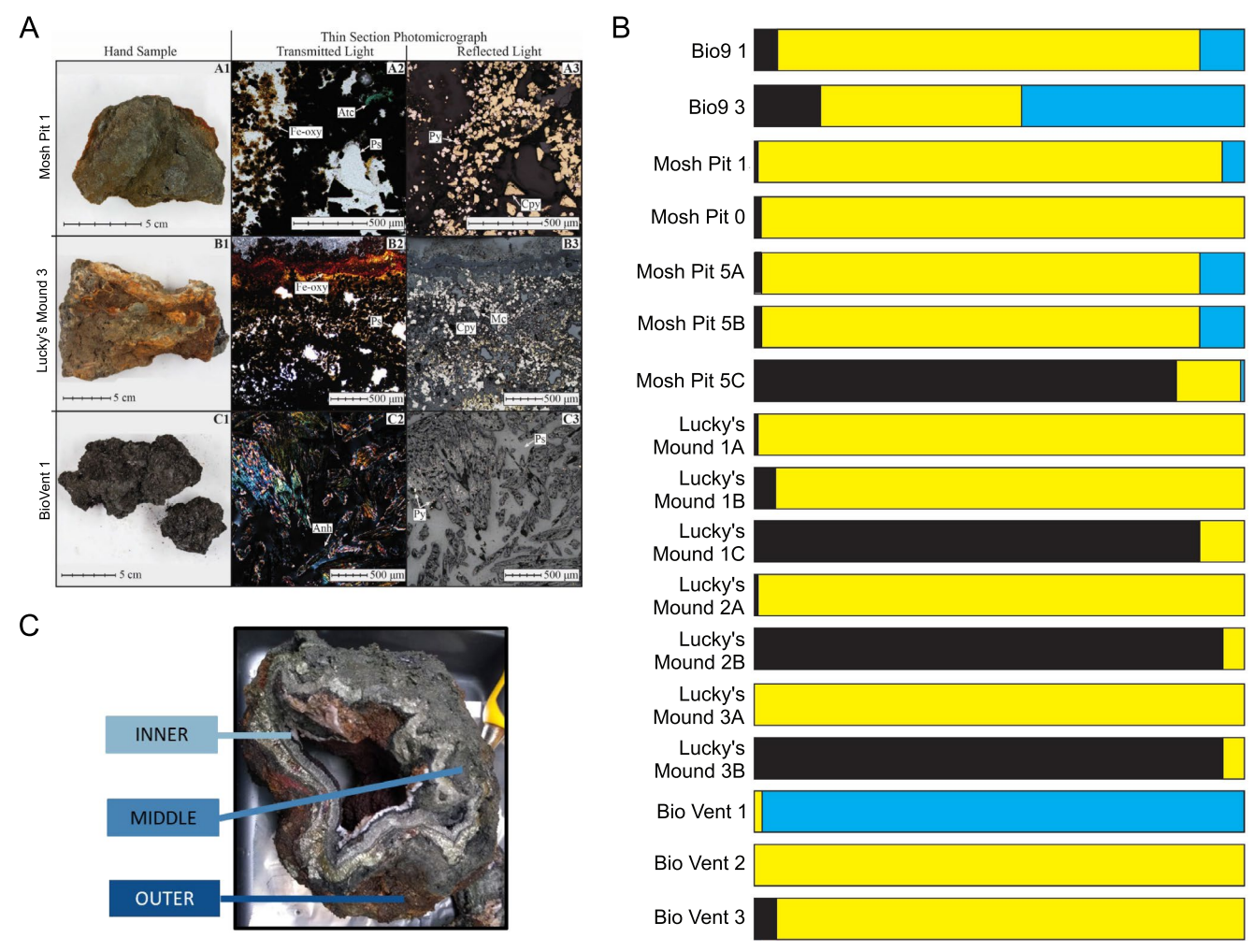
Carbon Fixation Pathway	Key Genes
Reverse TCA cycle	ATP-citrate lyase (aclAB)
CBB cycle	ribulose-bisphosphate carboxylase (rbcSL)
WL pathway	carbon-monoxide dehydrogenase (CooS, ascA)
2-HP bicycle	malonyl-CoA reductase / 3-hydroxypropionate dehydrogenase (mcr)
3-HP/4-HB	4-hydroxybutyryl-CoA dehydratase (abfD)

Extended Data Table 3 | Stable carbon isotopic composition (δ^{13} C) of the major polar lipid fatty acids (PLFA), analyzed as FAMEs (fatty acid methyl esters)

Location	Dive	Activity	TOC run #1	TOC run #2	C16:0 PLFA	C16:1 PLFA	C18:0 PLFA	C18:1 PLFA
Bio9	AL5015	Inactive*	-20.2	-20.6	-23.8		-25.7	
P Vent	AL5017	Active	-18.8	-18.4	-24.1		-25.9	
Mosh Pit	AL5019	Inactive	-17.3	-18.1	-27.4	-25.8	-24.4	-21.1
Mosh Pit	AL5019	Inactive	-16.6	-17.3	-27.5		-28.0	

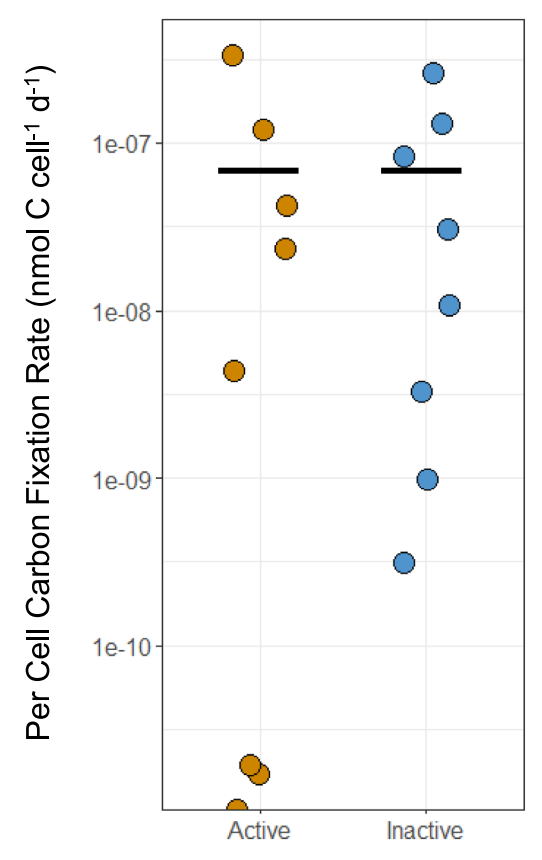
Extended Data Table 4 | Sample name reference table showing the original sample identifier assigned shipboard at the time of collection and the simplified sample identifier used in this manuscript

PVent 1 ALV5017-01-R010 PVent 2 ALV5017-01-R010 PVent 3 ALV5017-01-R010 Biol 1 ALV5017-01-R010 Biol 2 ALV5013-01-R018 Biol 3 ALV5015-01-R018 Biol 4 ALV5015-01-R018 Biol 5 ALV5015-01-R018 Biol 6 ALV5015-01-R018 Biol 9 ALV5014-08-R01 Biol Vent 1 ALV5014-08-R01 Biol Vent 2 ALV5014-08-R01 Biol Vent 3 ALV5014-08-R01 Mosh Pit 1 ALV5014-09-R01 Mosh Pit 2 ALV5014-09-R01 Mosh Pit 3 ALV5014-09-R01 Mosh Pit 3 ALV5014-09-R01 Mosh Pit 5 ALV5014-08-R01 Lucky S Mound 1 ALV5014-08-R01 Lucky S Mound 2 ALV5014-08-R01 Lucky S Mound 2 ALV5014-08-R01	Manuscript Sample ID	Assigned Shipboard Sample ID
PVent 3 ALV5017-01-R01D Bio9 1 ALV5013-01-R01C Bio9 2 ALV5013-01-R01B Bio9 3 ALV5015-01-R01A Bio9 4 ALV5015-01-R01B Bio9 5 ALV5015-01-R01C BioVent 1 ALV5046-08-R01 BioVent 2 ALV5046-08-R02 BioVent 3 ALV5046-09-R01 Mosh Pit 1 ALV5019-02-R01A Mosh Pit 2 ALV5019-02-R01A Mosh Pit 3 ALV5019-03-R01B Mosh Pit 4 ALV5019-03-R01A Mosh Pit 5 ALV5019-03-R01A Mosh Pit 5 ALV5019-03-R01B Mosh Pit 5 ALV5044-06-R01 Mosh Pit 58 ALV5044-06-R01 Mosh Pit 58 ALV5044-06-R01 Mosh Pit 58 ALV5044-06-R01 Luckys Mound 1 ALV5044-08-R01 Luckys Mound 18 ALV5044-08-R01 Luckys Mound 18 ALV5044-08-R01 Luckys Mound 2 ALV5045-02-R01 Luckys Mound 28 ALV5045-02-R01 Luckys Mound 28 ALV5045-02-R01 Luckys Mound 3 <td< td=""><td>P Vent 1</td><td>ALV5017-01-R01B</td></td<>	P Vent 1	ALV5017-01-R01B
Bio91 ALVS013-01-R016 Bio92 ALVS013-01-R018 Bio93 ALVS015-01-R01A Bio94 ALVS015-01-R018 Bio95 ALVS015-01-R016 BioVent 1 ALVS046-08-R01 BioVent 2 ALVS046-08-R02 BioVent 3 ALVS046-09-R01 Mosh Pit 1 ALVS046-09-R01 Mosh Pit 2 ALVS019-02-R01A Mosh Pit 3 ALVS019-02-R01A Mosh Pit 3 ALVS019-03-R01C Mosh Pit 3 ALVS019-03-R01A Mosh Pit 4 ALVS019-03-R01B Mosh Pit 5 ALVS019-03-R01B Mosh Pit 5 ALVS044-06-R01 Mosh Pit 5A ALVS044-06-R01 Mosh Pit 5C ALVS044-06-R01 Mosh Pit 5C ALVS044-06-R01 Luckys Mound 1 ALVS044-08-R01 Luckys Mound 18 ALVS044-08-R01 Luckys Mound 18 ALVS044-08-R01 Luckys Mound 2 ALVS045-02-R01 Luckys Mound 2A ALVS045-02-R01 Luckys Mound 2B ALVS045-02-R01 Luckys Mound 2B A	P Vent 2	ALV5017-01-R01C
Bio9 2	P Vent 3	ALV5017-01-R01D
Bio9 3 ALV5015-01-R01A Bio9 4 ALV5015-01-R01B Bio9 5 ALV5046-0R-R01 BioVent 1 ALV5046-08-R01 BioVent 2 ALV5046-09-R01 BioVent 3 ALV5046-09-R01 Mosh Pit 1 ALV5019-02-R01A Mosh Pit 2 ALV5019-02-R01C Mosh Pit 3 ALV5019-03-R01A Mosh Pit 4 ALV5019-03-R01B Mosh Pit 5 ALV5044-06-R01 Mosh Pit 5 ALV5044-06-R01 Mosh Pit 5 ALV5044-06-R01 Mosh Pit 5 ALV5044-06-R01 Mosh Pit 5 ALV5044-08-R01 Lucky's Mound 1 ALV5044-08-R01 Lucky's Mound 1 ALV5044-08-R01 Lucky's Mound 1A ALV5044-08-R01 Lucky's Mound 1B ALV5044-08-R01 Lucky's Mound 1C ALV5044-08-R01 Lucky's Mound 2 ALV5045-02-R01 Lucky's Mound 2A ALV5045-02-R01 Lucky's Mound 2B ALV5045-02-R01 Lucky's Mound 3 ALV5045-02-R01 Lucky's Mound 3A ALV5045-02-R01	Bio91	ALV5013-01-R01C
Bio9 4 ALVS015-01-R018 Bio9 5 ALVS015-01-R01C BioVent 1 ALVS046-08-R01 BioVent 2 ALVS046-08-R02 BioVent 3 ALVS046-09-R01 Mosh Pit 1 ALVS019-02-R01A Mosh Pit 2 ALVS019-02-R01C Mosh Pit 3 ALVS019-03-R01C Mosh Pit 4 ALVS019-03-R01B Mosh Pit 5 ALVS019-03-R01B Mosh Pit 5 ALVS044-06-R01 Mosh Pit 5A ALVS044-06-R01 Mosh Pit 5C ALVS044-06-R01 Mosh Pit 5C ALVS044-08-R01 Lucky's Mound 1 ALVS044-08-R01 Lucky's Mound 1A ALVS044-08-R01 Lucky's Mound 1B ALVS044-08-R01 Lucky's Mound 1C ALVS044-08-R01 Lucky's Mound 2 ALVS045-02-R01 Lucky's Mound 2A ALVS045-02-R01 Lucky's Mound 2B ALVS045-02-R01 Lucky's Mound 3 ALVS045-04-R01 Lucky's Mound 3A ALVS045-04-R01	Bio9 2	ALV5013-01-R01B
Bio9 5 ALV5015-01-R01C BioVent 1 ALV5046-08-R01 BioVent 2 ALV5046-08-R02 BioVent 3 ALV5046-09-R01 Mosh Pit 1 ALV5019-02-R01A Mosh Pit 2 ALV5019-02-R01C Mosh Pit 3 ALV5019-03-R01B Mosh Pit 3 ALV5019-03-R01B Mosh Pit 4 ALV5019-03-R01B Mosh Pit 5 ALV5044-06-R01 Mosh Pit 5A ALV5044-06-R01 Mosh Pit 5B ALV5044-06-R01 Mosh Pit 5C ALV5044-08-R01 Lucky's Mound 1 ALV5044-08-R01 Lucky's Mound 1A ALV5044-08-R01 Lucky's Mound 1B ALV5044-08-R01 Lucky's Mound 1C ALV5044-08-R01 Lucky's Mound 2 ALV5044-08-R01 Lucky's Mound 2 ALV5045-02-R01 Lucky's Mound 2A ALV5045-02-R01 Lucky's Mound 2B ALV5045-02-R01 Lucky's Mound 3 ALV5045-04-R01 Lucky's Mound 3 ALV5045-04-R01	Bio93	ALV5015-01-R01A
BioVent 1 ALV5046-08-R01 BioVent 2 ALV5046-08-R02 BioVent 3 ALV5046-09-R01 Mosh Pit 1 ALV5019-02-R01A Mosh Pit 2 ALV5019-02-R01C Mosh Pit 0 ALV5019-03-R01C Mosh Pit 3 ALV5019-03-R01A Mosh Pit 4 ALV5019-03-R01B Mosh Pit 5 ALV5044-06-R01 Mosh Pit 5A ALV5044-06-R01 Mosh Pit 5B ALV5044-06-R01 Mosh Pit 5C ALV5044-06-R01 Mosh Pit 5C ALV5044-08-R01 Lucky's Mound 1 ALV5044-08-R01 Lucky's Mound 1 ALV5044-08-R01 Lucky's Mound 1A ALV5044-08-R01 Lucky's Mound 1B ALV5044-08-R01 Lucky's Mound 1C ALV5044-08-R01 Lucky's Mound 2A ALV5045-02-R01 Lucky's Mound 2A ALV5045-02-R01 Lucky's Mound 2B ALV5045-02-R01 Lucky's Mound 3 ALV5045-02-R01 Lucky's Mound 3A ALV5045-02-R01	Bio9 4	ALV5015-01-R01B
BioVent 2 ALV5046-08-R02 BioVent 3 ALV5046-09-R01 Mosh Pit 1 ALV5019-02-R01A Mosh Pit 2 ALV5019-02-R01C Mosh Pit 0 ALV5019-03-R01C Mosh Pit 3 ALV5019-03-R01A Mosh Pit 4 ALV5019-03-R01B Mosh Pit 5 ALV5044-06-R01 Mosh Pit 5B ALV5044-06-R01 Mosh Pit 5C ALV5044-06-R01 Mosh Pit 5C ALV5044-08-R01 Lucky's Mound 1 ALV5044-08-R01 Lucky's Mound 1A ALV5044-08-R01 Lucky's Mound 1B ALV5044-08-R01 Lucky's Mound 1C ALV5044-08-R01 Lucky's Mound 2 ALV5045-02-R01 Lucky's Mound 2A ALV5045-02-R01 Lucky's Mound 2B ALV5045-02-R01 Lucky's Mound 3 ALV5045-04-R01	Bio9 5	ALV5015-01-R01C
BioVent 3 ALV5046-09-R01 Mosh Pit 1 ALV5019-02-R01A Mosh Pit 2 ALV5019-02-R01C Mosh Pit 0 ALV5019-03-R01C Mosh Pit 3 ALV5019-03-R01A Mosh Pit 4 ALV5019-03-R01B Mosh Pit 5 ALV5044-06-R01 Mosh Pit 5A ALV5044-06-R01 Mosh Pit 5B ALV5044-06-R01 Mosh Pit 5C ALV5044-08-R01 Lucky's Mound 1 ALV5044-08-R01 Lucky's Mound 1A ALV5044-08-R01 Lucky's Mound 1B ALV5044-08-R01 Lucky's Mound 1C ALV5044-08-R01 Lucky's Mound 2 ALV5045-02-R01 Lucky's Mound 2A ALV5045-02-R01 Lucky's Mound 2B ALV5045-02-R01 Lucky's Mound 3 ALV5045-04-R01 Lucky's Mound 3 ALV5045-04-R01	BioVent 1	ALV5046-08-R01
Mosh Pit 1 ALV5019-02-R01C Mosh Pit 0 ALV5019-03-R01C Mosh Pit 3 ALV5019-03-R01A Mosh Pit 4 ALV5019-03-R01B Mosh Pit 5 ALV5044-06-R01 Mosh Pit 5A ALV5044-06-R01 Mosh Pit 5B ALV5044-06-R01 Mosh Pit 5C ALV5044-06-R01 Luckys Mound 1 ALV5044-08-R01 Luckys Mound 1A ALV5044-08-R01 Luckys Mound 1B ALV5044-08-R01 Luckys Mound 1C ALV5044-08-R01 Luckys Mound 2 ALV5044-08-R01 Luckys Mound 2A ALV5045-02-R01 Luckys Mound 2B ALV5045-02-R01 Luckys Mound 3 ALV5045-02-R01 Luckys Mound 3 ALV5045-02-R01	BioVent 2	ALV5046-08-R02
Mosh Pit 2 ALV5019-02-R01C Mosh Pit 0 ALV5019-03-R01C Mosh Pit 3 ALV5019-03-R01A Mosh Pit 4 ALV5019-03-R01B Mosh Pit 5 ALV5044-06-R01 Mosh Pit 5A ALV5044-06-R01 Mosh Pit 5B ALV5044-06-R01 Mosh Pit 5C ALV5044-06-R01 Lucky's Mound 1 ALV5044-08-R01 Lucky's Mound 1A ALV5044-08-R01 Lucky's Mound 1B ALV5044-08-R01 Lucky's Mound 1C ALV5044-08-R01 Lucky's Mound 2 ALV5045-02-R01 Lucky's Mound 2A ALV5045-02-R01 Lucky's Mound 2B ALV5045-02-R01 Lucky's Mound 3 ALV5045-04-R01	BioVent 3	ALV5046-09-R01
Mosh Pit 0 ALV5019-03-R01C Mosh Pit 3 ALV5019-03-R01B Mosh Pit 4 ALV5019-03-R01B Mosh Pit 5 ALV5044-06-R01 Mosh Pit 5A ALV5044-06-R01 Mosh Pit 5B ALV5044-06-R01 Mosh Pit 5C ALV5044-06-R01 Lucky's Mound 1 ALV5044-08-R01 Lucky's Mound 1A ALV5044-08-R01 Lucky's Mound 1B ALV5044-08-R01 Lucky's Mound 2 ALV5044-08-R01 Lucky's Mound 2 ALV5045-02-R01 Lucky's Mound 2B ALV5045-02-R01 Lucky's Mound 3 ALV5045-04-R01 Lucky's Mound 3 ALV5045-04-R01	Mosh Pit 1	ALV5019-02-R01A
Mosh Pit 3 ALV5019-03-R01B Mosh Pit 4 ALV504-06-R01 Mosh Pit 5 ALV5044-06-R01 Mosh Pit 5A ALV5044-06-R01 Mosh Pit 5B ALV5044-06-R01 Mosh Pit 5C ALV5044-06-R01 Lucky's Mound 1 ALV5044-08-R01 Lucky's Mound 1A ALV5044-08-R01 Lucky's Mound 1B ALV5044-08-R01 Lucky's Mound 1C ALV5044-08-R01 Lucky's Mound 2 ALV5045-02-R01 Lucky's Mound 2A ALV5045-02-R01 Lucky's Mound 2B ALV5045-02-R01 Lucky's Mound 3 ALV5045-04-R01 Lucky's Mound 3A ALV5045-04-R01	Mosh Pit 2	ALV5019-02-R01C
Mosh Pit 4 ALV5019-03-R01B Mosh Pit 5 ALV5044-06-R01 Mosh Pit 5A ALV5044-06-R01 Mosh Pit 5B ALV5044-06-R01 Mosh Pit 5C ALV5044-08-R01 Lucky's Mound 1 ALV5044-08-R01 Lucky's Mound 1A ALV5044-08-R01 Lucky's Mound 1B ALV5044-08-R01 Lucky's Mound 1C ALV5044-08-R01 Lucky's Mound 2 ALV5045-02-R01 Lucky's Mound 2A ALV5045-02-R01 Lucky's Mound 2B ALV5045-02-R01 Lucky's Mound 3 ALV5045-04-R01 Lucky's Mound 3A ALV5045-04-R01	Mosh Pit O	ALV5019-03-R01C
Mosh Pit 5 ALV5044-06-R01 Mosh Pit 5B ALV5044-06-R01 Mosh Pit 5C ALV5044-06-R01 Lucky's Mound 1 ALV5044-08-R01 Lucky's Mound 1A ALV5044-08-R01 Lucky's Mound 1B ALV5044-08-R01 Lucky's Mound 2 ALV5044-08-R01 Lucky's Mound 2 ALV5045-02-R01 Lucky's Mound 2A ALV5045-02-R01 Lucky's Mound 2B ALV5045-02-R01 Lucky's Mound 3 ALV5045-04-R01 Lucky's Mound 3A ALV5045-04-R01	Mosh Pit 3	ALV5019-03-R01A
Mosh Pit 5A ALV5044-06-R01 Mosh Pit 5B ALV5044-06-R01 Mosh Pit 5C ALV5044-06-R01 Lucky's Mound 1 ALV5044-08-R01 Lucky's Mound 1A ALV5044-08-R01 Lucky's Mound 1B ALV5044-08-R01 Lucky's Mound 1C ALV5044-08-R01 Lucky's Mound 2 ALV5045-02-R01 Lucky's Mound 2A ALV5045-02-R01 Lucky's Mound 2B ALV5045-02-R01 Lucky's Mound 3 ALV5045-04-R01 Lucky's Mound 3A ALV5045-04-R01	Mosh Pit 4	ALV5019-03-R01B
Mosh Pit 5B ALV5044-06-R01 Mosh Pit 5C ALV5044-08-R01 Lucky's Mound 1 ALV5044-08-R01 Lucky's Mound 1A ALV5044-08-R01 Lucky's Mound 1B ALV5044-08-R01 Lucky's Mound 1C ALV5044-08-R01 Lucky's Mound 2 ALV5045-02-R01 Lucky's Mound 2A ALV5045-02-R01 Lucky's Mound 2B ALV5045-02-R01 Lucky's Mound 3 ALV5045-04-R01 Lucky's Mound 3A ALV5045-04-R01	Mosh Pit 5	ALV5044-06-R01
Mosh Pit 5C ALV5044-06-R01 Lucky's Mound 1 ALV5044-08-R01 Lucky's Mound 1A ALV5044-08-R01 Lucky's Mound 1B ALV5044-08-R01 Lucky's Mound 1C ALV5044-08-R01 Lucky's Mound 2 ALV5045-02-R01 Lucky's Mound 2A ALV5045-02-R01 Lucky's Mound 2B ALV5045-02-R01 Lucky's Mound 3 ALV5045-04-R01 Lucky's Mound 3A ALV5045-04-R01	Mosh Pit 5A	ALV5044-06-R01
Lucky's Mound 1 ALV5044-08-R01 Lucky's Mound 1B ALV5044-08-R01 Lucky's Mound 1C ALV5044-08-R01 Lucky's Mound 2 ALV5045-02-R01 Lucky's Mound 2A ALV5045-02-R01 Lucky's Mound 2B ALV5045-02-R01 Lucky's Mound 3 ALV5045-04-R01 Lucky's Mound 3A ALV5045-04-R01	Mosh Pit 5B	ALV5044-06-R01
Lucky's Mound 1A ALV5044-08-R01 Lucky's Mound 1B ALV5044-08-R01 Lucky's Mound 1C ALV5044-08-R01 Lucky's Mound 2 ALV5045-02-R01 Lucky's Mound 2A ALV5045-02-R01 Lucky's Mound 2B ALV5045-02-R01 Lucky's Mound 3 ALV5045-04-R01 Lucky's Mound 3A ALV5045-04-R01	Mosh Pit 5C	ALV5044-06-R01
Lucky's Mound 1B ALV5044-08-R01 Lucky's Mound 1C ALV5044-08-R01 Lucky's Mound 2 ALV5045-02-R01 Lucky's Mound 2A ALV5045-02-R01 Lucky's Mound 2B ALV5045-02-R01 Lucky's Mound 3 ALV5045-04-R01 Lucky's Mound 3A ALV5045-04-R01	Lucky's Mound 1	ALV5044-08-R01
Lucky's Mound 1C ALV5044-08-R01 Lucky's Mound 2 ALV5045-02-R01 Lucky's Mound 2A ALV5045-02-R01 Lucky's Mound 2B ALV5045-02-R01 Lucky's Mound 3 ALV5045-04-R01 Lucky's Mound 3A ALV5045-04-R01	Lucky's Mound 1A	ALV5044-08-R01
Lucky's Mound 2 ALV5045-02-R01 Lucky's Mound 2A ALV5045-02-R01 Lucky's Mound 2B ALV5045-02-R01 Lucky's Mound 3 ALV5045-04-R01 Lucky's Mound 3A ALV5045-04-R01	Lucky's Mound 1B	ALV5044-08-R01
Lucky's Mound 2A ALV5045-02-R01 Lucky's Mound 2B ALV5045-02-R01 Lucky's Mound 3 ALV5045-04-R01 Lucky's Mound 3A ALV5045-04-R01	Lucky's Mound 1C	ALV5044-08-R01
Lucky's Mound 2B ALV5045-02-R01 Lucky's Mound 3 ALV5045-04-R01 Lucky's Mound 3A ALV5045-04-R01	Lucky's Mound 2	ALV5045-02-R01
Lucky's Mound 3 ALV5045-04-R01 Lucky's Mound 3A ALV5045-04-R01	Lucky's Mound 2A	ALV5045-02-R01
Lucky's Mound 3A ALV5045-04-R01	Lucky's Mound 2B	ALV5045-02-R01
	Lucky's Mound 3	ALV5045-04-R01
Lucky's Mound 3B ALV5045-04-R01	Lucky's Mound 3A	ALV5045-04-R01
	Lucky's Mound 3B	ALV5045-04-R01

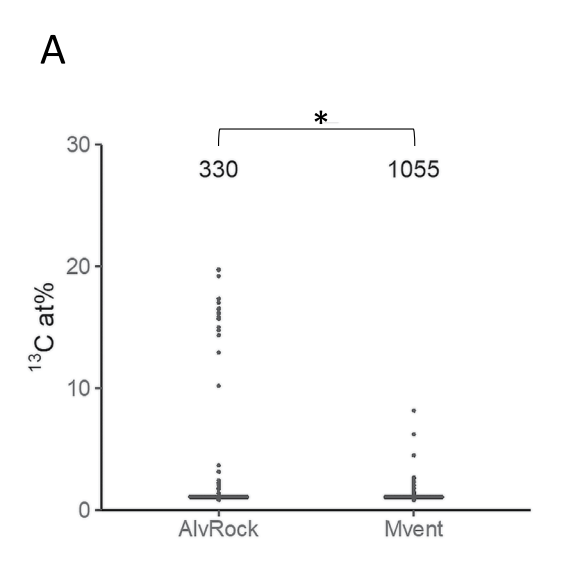


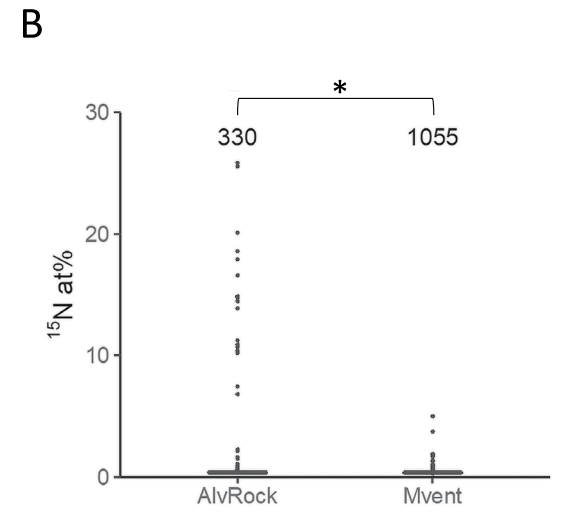
Extended Data Fig. 1 | **a**, Representative samples collected from inactive and active hydrothermal vent deposits including photographs of bulk samples (A1-C1) as well as thin section micrographs viewed with transmitted (A2-C2) and reflected light (A3-C3); Anh, anhydrite; Atc, atacamite; Cpy, chalcopyrite; Fe-oxy, iron oxyhydroxide; Mc, marcasite, Py, pyrite; Ps, pore space. **b**, Bulk minerology

of samples. Black denotes iron oxyhydroxides, Yellow denotes sulfides, and Blue denotes sulfates. \mathbf{c} , Photograph of representative subdivided inactive vent sample from Lucky's Mound used in carbon assimilation assays showing the three regions of interest (inner conduit, middle region, and outer crust).



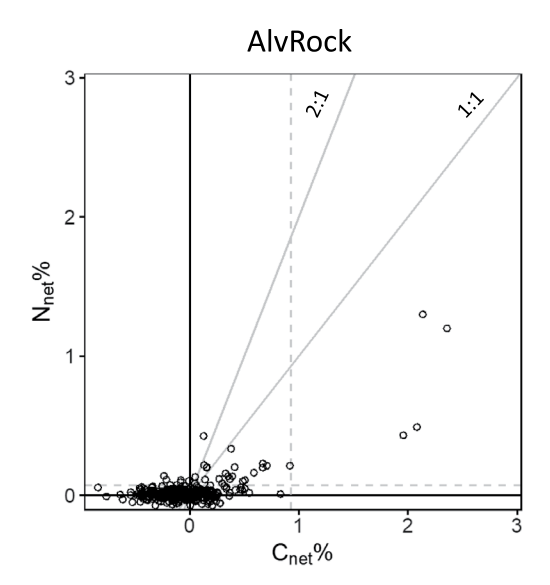
 $\textbf{Extended Data Fig. 2} | Assimilation of \ ^{14}C-bicarbonate by microbial communities (shown in Fig. 1) from active (n = 8; biologically independent samples) and inactive (n = 8) hydrothermal vent deposits, normalized for cell abundance (Extended Data Table 1). Black line indicated mean value.$



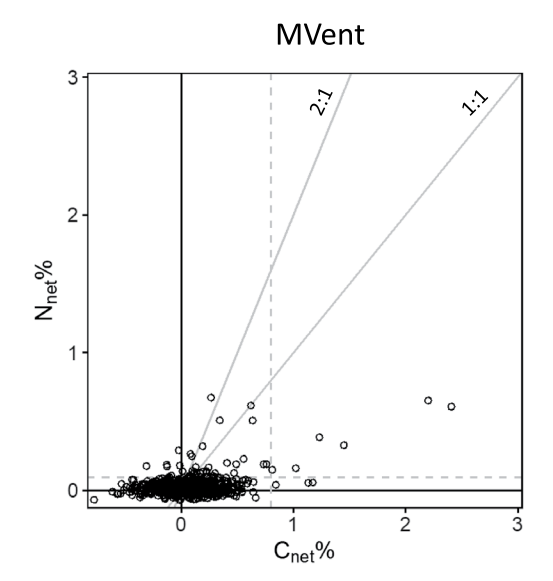


Extended Data Fig. 3 | NanoSIMS comparison of uptake of 13 C-bicarbonate **a**, and 15 N-ammonium **b**, in individual cells (gray dots) from a single rock sample at each of AlvinellidRock (active vent deposit) and Mvent (inactive vent deposit) after 2 days of incubation. Box plots indicating the median, upper, and lower quartiles (but, appearing as lines due to mostly low activity/inactive cells) are

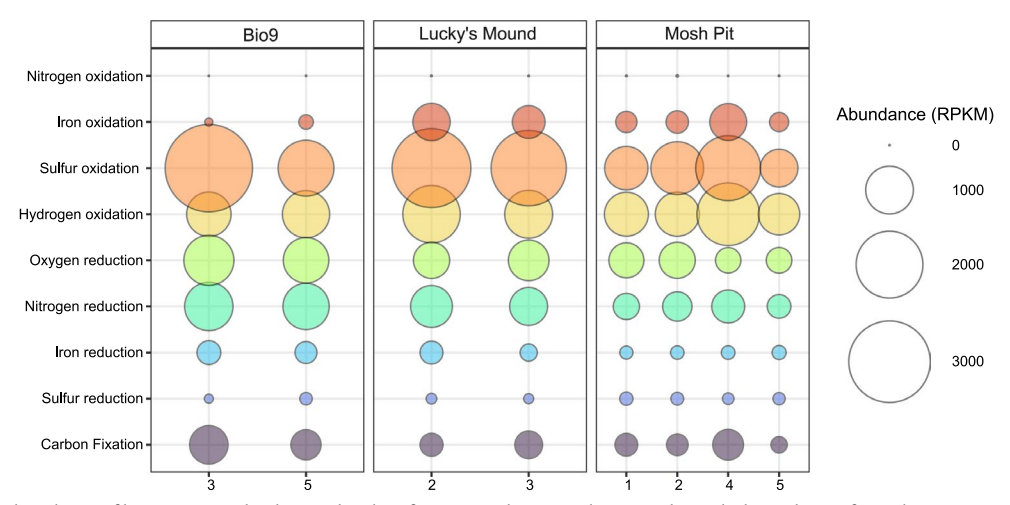
overlaid in black. Numbers above the plots indicate the number of regions of interest (putative cells) analyzed, and asterisks indicate a statistically significant difference (p < 0.05) using a two-sided, Mann-Whitney (MW) test with a Bonferroni correction for multiple hypotheses.



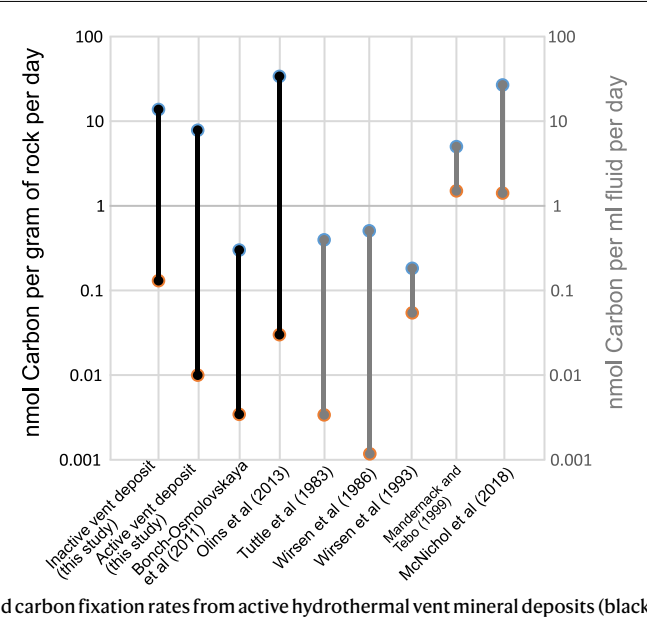
 $\label{lem:continuous} \textbf{Extended Data Fig. 4} \ | \ Relative uptake of 13C-bicarbonate and 15N-ammonium in individual cells (black circles) measured by nanoSIMS from AlvinellidRock (active vent deposit) and Mvent (inactive vent deposit) after 2 days of incubation. Data is replotted from main text Fig. 3 with truncated axes to better display data points around the origin (lower activity cells). Based on their relative assimilation of$



each substrate, the regions below the 2:1 line include chemoautotrophic cells, the region above the 2:1 line includes heterotrophic cells, and the regions to the left (x-axis) or below (y-axis) the dashed lines include cells below the detection limit of uptake for that substrate. Regions are defined as in Dekas et al. 41 .



 $\textbf{Extended Data Fig. 5} | Abundance of key genes involved in total carbon fixation pathways and potential metabolic pathways for redox reactions annotated based on HMMs using MagicLamp^{72} (Supplementary Table 1).$



Extended Data Fig. 6 | Summary of published carbon fixation rates from active hydrothermal vent mineral deposits (black; right-axis) and hydrothermal vent fluids (grey; left-axis). The blue and orange dots denote the highest and lowest reported rates, respectively.

nature portfolio

Amanda Achberger

Corresponding author(s): Jason Sylvan

Last updated by author(s): Jul 27, 2023

Reporting Summary

Nature Portfolio wishes to improve the reproducibility of the work that we publish. This form provides structure for consistency and transparency in reporting. For further information on Nature Portfolio policies, see our <u>Editorial Policies</u> and the <u>Editorial Policy Checklist</u>.

For all statistical analyses, confirm that the following items are present in the figure legend, table legend, main text, or Methods section.

~					
< ⋅	トつ	+1	ıct	- 1.	Γ S
٠,			ואו	- 1	1 >

n/a	Confirmed
	The exact sample size (n) for each experimental group/condition, given as a discrete number and unit of measurement
	A statement on whether measurements were taken from distinct samples or whether the same sample was measured repeatedly
	The statistical test(s) used AND whether they are one- or two-sided Only common tests should be described solely by name; describe more complex techniques in the Methods section.
\boxtimes	A description of all covariates tested
	A description of any assumptions or corrections, such as tests of normality and adjustment for multiple comparisons
	A full description of the statistical parameters including central tendency (e.g. means) or other basic estimates (e.g. regression coefficient) AND variation (e.g. standard deviation) or associated estimates of uncertainty (e.g. confidence intervals)
	For null hypothesis testing, the test statistic (e.g. <i>F</i> , <i>t</i> , <i>r</i>) with confidence intervals, effect sizes, degrees of freedom and <i>P</i> value noted Give <i>P</i> values as exact values whenever suitable.
\boxtimes	For Bayesian analysis, information on the choice of priors and Markov chain Monte Carlo settings
\boxtimes	For hierarchical and complex designs, identification of the appropriate level for tests and full reporting of outcomes
\boxtimes	Estimates of effect sizes (e.g. Cohen's d, Pearson's r), indicating how they were calculated
	Our web collection on statistics for biologists contains articles on many of the points above.

Software and code

Policy information about availability of computer code

Data collection

no software was used.

Data analysis

Image analysis for NanoSIMS was performed with Look@NanoSIMS software. Isodat Gas Isotope Ratio MS Software (v3.0.94.12) was used for data processing of TOC data while Bruker Compass Data Analysis software (v4.4) and XCalibur (v4.1.50) was used for data processing of lipid data. The following open source code/programs were used for analysis of metagenomic data: Trimmomatic (v0.39), Megahit (v1.2.9), Prodigal (v2.6.3), Bowtie2 (v2.5.0), MMSeqs2, GhostKoala (v2.0), and MagicLamp (version unspecified).

For manuscripts utilizing custom algorithms or software that are central to the research but not yet described in published literature, software must be made available to editors and reviewers. We strongly encourage code deposition in a community repository (e.g. GitHub). See the Nature Portfolio guidelines for submitting code & software for further information.

Data

Policy information about availability of data

All manuscripts must include a data availability statement. This statement should provide the following information, where applicable:

- Accession codes, unique identifiers, or web links for publicly available datasets
- A description of any restrictions on data availability
- For clinical datasets or third party data, please ensure that the statement adheres to our policy

Raw metagenomic data are available in the NCBI Sequence Read Archive (SRA) under BioProject PRJNA998752.

Research involving human participants, their data, or biological material

Policy information about stu and sexual orientation and <u>r</u>	dies with <u>human participants or human data</u> . See also policy information about <u>sex, gender (identity/presentation),</u> ace, ethnicity and racism.
Reporting on sex and gend	der N/A
Reporting on race, ethnicity other socially relevant groupings	ty, or N/A
Population characteristics	N/A
Recruitment	N/A
Ethics oversight	N/A
Note that full information on th	e approval of the study protocol must also be provided in the manuscript.
Field-specific	reporting
Please select the one below	that is the best fit for your research. If you are not sure, read the appropriate sections before making your selection.
Life sciences	Behavioural & social sciences Ecological, evolutionary & environmental sciences
or a reference copy of the docume	nt with all sections, see <u>nature.com/documents/nr-reporting-summary-flat.pdf</u>
Ecological, ev	olutionary & environmental sciences study design
All studies must disclose on	these points even when the disclosure is negative.
,	This study primarily examined the inorganic carbon fixation rates of rock-hosted microbial communities from actively venting and inactive hydrothermal chimneys from the East Pacific Rise at the segment located at ~9°50'N. To perform this analysis, 7 active hydrothermal vent deposits and 12 inactive deposits were incubated at 65°C or 4°C, respectively, in the presence of 14C-bicarbonate Additionally, one active and one inactive deposit sample each were similarly incubated in the presence of 13C-bicarbonate and 15N-ammonium for single-cell uptake experiments and analysis with nanoscale secondary ion mass spectrometry. An analysis of stable carbon isotopic composition (delta 13C) of total organic carbon (TOC) and polar lipid fatty acids measured as FAMEs (fatty acid methyl esters) was also performed on 2 active and 3 inactive hydrothermal vent deposit samples to elucidate the potential carbon fixation pathways being utilized by the microbial community. This was further expanded upon by a metagenomic analysis of 8 inactive hydrothermal deposit samples. From this metagenomic analysis, the prevalence of potential carbon fixation pathways were described as were the taxonomic affiliation of the organisms associated with the pathways.
'	For this study, hydrothermal vent mineral deposits were collected from the East Pacific Rise (EPR) 9°50′ N ridge spreading region to examine the inorganic carbon fixation potential of associated microbial communities. In this region, samples were collected from chimneys actively venting high temperature hydrothermal fluid as well as chimneys with no detectable fluid flow to evaluate the full range of primary productivity potential along this region of the EPR.
	Samples were collected from active and inactive vent chimneys at East Pacific Rise crest 9°50 N during three field expeditions: by Human Occupied Vehicle (HOV) Alvin on the AT42-09 cruise in April 2019 and in December 2019 on the AT42-21 cruise, both on R/V Atlantis, and by Remotely Operated Vehicle (ROV) Jason in April 2021 on the RR2102 cruise on the R/V Roger Revelle. Sample sizes were dictated by dive time and ability to recover samples due to the limitations of deep sea work.
	Carbon fixation rates as determined based on 14C-bicarbonate incorporation and measured via Liquid Scintillation were collected and recorded by Amanda Achberger and Jason Sylvan. Metagenomic analysis was performed by Amanda Achberger. Cell enumeration counts were determined via microscopy and collected by Charles Holmes III. The single-cell uptake incorporation of 13C-bicarbonate and 15N-ammonium and subsequent analysis with nanoscale secondary ion mass spectrometry was conducted by Charles Holmes III and Rose Jones (at-sea incubations) and Nicolette Meyer and Anne Dekas (sample processing and data analysis). Samples for stable carbon isotopic composition (delta 13C) of total organic carbon and polar lipid fatty acids were collected at sea by Eoghan Reeves and Jonas Brüenjes and processed and analyzed in the laboratory by Florence Schubotz and Alex Manthey. Petrographic analysis was performed by Sarah Moriarty and John Jamieson.
	Samples were collected from active and inactive vent chimneys at East Pacific Rise crest 9°50 N during three field expeditions: by Human Occupied Vehicle (HOV) Alvin on the AT42-09 cruise in April 2019 and in December 2019 on the AT42-21 cruise, both on R/V Atlantis, and by Remotely Operated Vehicle (ROV) Jason in April 2021 on the RR2102 cruise on the R/V Roger Revelle. Samples were collected as cruise and dive times allowed.
Data exclusions	No data were exluded
Reproducibility	For inorganic carbon fixation rate experiments, 2-3 replicates were performed for each sample analyzed. All replicates were included

Reproducibility	(in the analysis. For all other experiments, replication was either not applicable or not performed.			
Randomization	Randomization is not applicable to this study because it focused on examining differences between discreet hydrothermal vent types based on geological characteristics.			
Blinding	Blinding is not applicable to the study because it focused on examining differences between discreet hydrothermal vent types based on geological characteristics.			
Did the study involve fiel	d work? Xes No			
ield work, collec	tion and transport			
Field conditions	Samples were collected from active (temperature range 280-300C) and inactive (2-4C) vent chimneys at East Pacific Rise crest 9°50 N during three field expeditions: by Human Occupied Vehicle (HOV) Alvin on the AT42-09 cruise in April 2019 and in December 2019 on the AT42-21 cruise, both on R/V Atlantis, and by Remotely Operated Vehicle (ROV) Jason in April 2021 on the RR2102 cruise on the R/V Roger Revelle.			
Location	Collection occurred in the Pacific Ocean at the East Pacific Rise crest 9°50 N at an average depth of 2500 meters below sea surface.			
Access & import/export	Sampling occurred in international waters at the East Pacific Rise crest 9°50 N, therefore no permits were required as there is no national jurisdiction. No international laws exist for the kind of sampling done for this study. Sampling required several research vessel cruises as well use of Human Occupied and Remotely Operated Vehicles.			
Disturbance	Sampling of hydrothermal vent chimneys were performed with the manipulatory arms of Human Occupied and Remotely Operated Vehicles. This method of collection is challenging, however, care was taken to remove only small sections of the chimney and limit			

Reporting for specific materials, systems and methods

We require information from authors about some types of materials, experimental systems and methods used in many studies. Here, indicate whether each material, system or method listed is relevant to your study. If you are not sure if a list item applies to your research, read the appropriate section before selecting a response.

Materials & experimental systems	Methods		
n/a Involved in the study	n/a Involved in the study		
Antibodies	ChIP-seq		
Eukaryotic cell lines	Flow cytometry		
Palaeontology and archaeology	MRI-based neuroimaging		
Animals and other organisms	·		
Clinical data			
Dual use research of concern			
Plants			

disruption to the overall structure when possible.